THERMAL-HYDROLOGICAL-MECHANICAL MODELING OF A SATURATED CLAY SHALE REPORT ON HE-D TEST MODELING

Prepared for

U.S. Nuclear Regulatory Commission
Contract No. NRC–HQ–12–C–02–0089

Prepared by

Goodluck Ofoegbu,[1] Biswajit Dasgupta,[1]
Chandrika Manepally,[1] and Randall Fedors[2]

[1]Center for Nuclear Waste Regulatory Analyses
San Antonio, Texas

[2]U.S. Nuclear Regulatory Commission
Washington, DC

April 2015

ABSTRACT

This report describes the status of numerical modeling performed as part of participation by the U.S. Nuclear Regulatory Commission (NRC) and the Center for Nuclear Waste Regulatory Analyses (CNWRA®) in Task B1 of the **De**velopment of **Co**upled Models and Their **Val**idation Against **Ex**periments (DECOVALEX) 2015 project. The modeling described in this report focuses on Step 1 of Task B1, which examines thermal-hydrological-mechanical (THM) processes relevant to the response of an argillaceous rock mass (known as the Opalinus Clay) to several months of heating from a buried cylindrical heat source. The experiment, referred to as the HE-D test, was conducted at the Mont Terri Underground Research Laboratory in Switzerland. The Opalinus Clay is an indurated rock formation. Later steps for Task B1 will include modeling to characterize the behavior of bentonite in a laboratory column test, and modeling the HE-E *in situ* thermal experiment that integrates bentonite and host rock thermal-hydrological-mechanical behavior. Several groups, including NRC, participated in the modeling exercise under DECOVALEX 2015 Task B1, which has an over-all objective of understanding the THM processes that may be important to the performance of a nuclear waste disposal design that includes an argillaceous host rock with or without a bentonite buffer.

The NRC/CNWRA team modeled the HE-D test using FLAC, a commercially available computer code that is widely used for geomechanical modeling. This report describes the status of numerical modeling and compares the calculated results against field measurements. Insights from modeling of the host-rock of the HE-D test will be applied to later modeling step in Task B1 of the host-rock component of the HE-E test.

The calculated rock temperature generally captures the evolution of temperature at several monitored locations. Analysis of the calculated and measured temperature histories indicates that the layered nature of the Opalinus Clay likely caused an important effect on the measured response. A difference in the thermal conductivity of the host rock in bed-normal and bed-parallel directions could explain differences between the calculated and measured temperature histories. A sensitivity analysis of the effects of thermal conductivity on the calculated temperature suggests a bed-normal thermal conductivity smaller than 1.77 W/m.K and a bed-parallel thermal conductivity greater than 2.8 W/m.K.

The calculated pore pressure shows sensitivity to the thermal conductivity: a smaller thermal conductivity results in a greater temperature and, hence, greater pore pressure. Additionally, the calculated pore pressure increased as permeability decreased. This sensitivity of calculated pore pressure to permeability suggests that permeability anisotropy illustrated as a difference between the bed-normal and bed-parallel permeability could explain some of the differences between the calculated and measured pore pressures.

Calculated deformations indicate that the heating caused the host rock to expand. Generally, the calculated expansion increased with distance from the heater to a maximum value and decreased with distance thereafter. However, the magnitude of measured rock strain is generally greater than the magnitude of calculated strain. The authors did not try to resolve the difference between the calculated and measured mechanical responses but instead focused on understanding the thermal and hydrological (TH) responses. Because the TH effect on mechanical response is expected to be stronger than the mechanical effect on the TH response, an effort to resolve the mechanical response would be more fruitful after resolving the TH responses satisfactorily. As discussed previously, analyses of the TH responses indicated that changing the model geometry to allow explicit representation of different bed-normal and bed-parallel thermal and hydraulic conductivities could result in matching the measured TH

responses more closely. However, pending implementation of anisotropic capabilities in the modeling tool, the authors expected sufficient understanding would be obtained of the TH behavior of the host-rock to proceed with HE-E test modeling in the third step of Task B1 where THM effects in the host rock are secondary to THM effects in the bentonite buffer.

This numerical modeling of the HE-D heater test provided an in-depth understanding of the THM behavior of the Opalinus Clay. Study results indicate that the anisotropy of thermal and hydrological properties (i.e., thermal and hydraulic conductivities in bed-parallel directions differ from the bed-normal conductivities) likely play an important role in the THM behavior of the Opalinus Clay. This conclusion will be evaluated in the context of the HE-E test that focuses on THM behavior of the buffer and its interaction with the host rock.

CONVERSION FACTORS

Name	SI Unit	Conversion
Density	1 kg/m^3	= 0.06243 lb_m/ft^3
Heat transfer rate	1 W	= 3.4123 Btu/h
Length	1 m	= 39.370 in
Power	1 W	= 3.412 Btu/h
Pressure and Stress*	1 N/m^2 (1 Pa)	= 0.000145 psi
Specific heat	1 kJ/Kg.K	= 0.2389 $Btu/lb_m.°F$
Thermal conductivity	1 W/m.K	= 0.57782 Btu/h.ft.°F
Viscosity (dynamic)†	1 $N.s/m^2$	= 5.8016×10^{-6} $lb_f.h/ft^2$
Physical Constants		
Gravitational Acceleration (Sea Level)		g = 9.807 m/s^2 = 32.174 ft/s^2

*The SI name for the quantity pressure is Pascal (Pa) having units N/m^2 or $Kg/m.s^2$

†Also expressed in equivalent units of kg/s.m

CONTENTS

FIGURES

FIGURES (Continued)

TABLES

ACKNOWLEDGMENTS

This report was prepared to document work performed by the Center for Nuclear Waste Regulatory Analyses (CNWRA®) for the U.S. Nuclear Regulatory Commission (NRC) under Contract No. NRC–HQ–12–C–02–0089. The studies and analyses reported here were performed on behalf of the NRC Office of Nuclear Material Safety and Safeguards, Division of Spent Fuel Alternative Strategies. The report is an independent product of CNWRA and does not necessarily reflect the views or regulatory position of NRC.

The authors thank Stuart Stothoff for technical review and Gordon Wittmeyer for programmatic reviews. The authors also thank Arturo Ramos for support in report preparation and Lauren Mulverhill for editorial review. The authors also gratefully acknowledged Agence nationale pour la gestion des déchets radioactifs (ANDRA) who was leading the project management of the HE-D experiment and produced all measurements presented in this report.

QUALITY OF DATA, ANALYSES, AND CODE DEVELOPMENT

DATA: All CNWRA-generated original data contained in this report meet quality assurance requirements described in the Geosciences and Engineering Division Quality Assurance Manual. Sources of other data should be consulted for determining the level of quality of those data. The work presented in this report is document in Scientific Notebook Nos. 1103E (Ofoegbu and Dasgupta, 2013) and 1611E (Manepally, 2013).

ANALYSES AND CODES: The computer software used is FLAC (Itasca Consulting Group, 2011). FLAC is a commercial software controlled under TOP–18. Documentation for the calculations can be found in Scientific Notebooks 1103E (Ofoegbu and Dasgupta, 2013) and 1137E (Manepally, 2013).

REFERENCES

Itasca Consulting Group. "FLAC V 7.0, Fast Lagrangian Analysis of Continua, User's Guide." Minneapolis, Minnesota: Itasca Consulting Group. 2011.

Manepally, C. "ISFR Task Order 9 Decovalex-Related Activities." Scientific Notebook No. 1611E. San Antonio, Texas: Center for Nuclear Waste Regulatory Analyses. 2013.

Ofoegbu, G.I. and B. Dasgupta. "Development of Constitutive Relations for Unsaturated Soil and Thermal-Hydrological-Mechanical Coupling." Scientific Notebook No. 1103E. San Antonio, Texas: Center for Nuclear Waste Regulatory Analyses. pp. 86–112. 2013.

1 INTRODUCTION

The **De**velopment of **Co**upled Models and Their **Val**idation Against **Ex**periments (DECOVALEX) project is an international collaboration focused on modeling thermal-hydrological-mechanical-chemical (THMC) processes associated with the deep geologic disposal of high-level radioactive waste and spent nuclear fuel[1]. The U.S. Nuclear Regulatory Commission (NRC) is a participant in the current 3.5-year phase, DECOVALEX-2015, and is supported by staff from the Center for Nuclear Waste Regulatory Analyses (CNWRA®) on Task B1 (HE-E experiment) of the collaboration. The NRC joined DECOVALEX-2015 project to leverage international experience to improve the modeling capabilities for disposal in clay host rocks that may include bentonite buffers, and to develop software tools appropriate for these domains.

Task B1 of DECOVALEX-2015 is geared towards understanding the thermal-hydrological-mechanical (THM) processes in a bentonite buffer and argillaceous host rock at the Mont Terri Underground Research Laboratory (URL), Switzerland (Figure 1-1). The task is based on three tests

(1) HE-D heating test at Mont Terri (rock only)
(2) Laboratory column tests on bentonite pellets (used as a buffer for the HE-E test)
(3) HE-E heating experiment at Mont Terri (integrating buffer materials and host rock)

This report provides the status of staff's analyses for the first step, simulating the THM behavior in the host rock of the HE-D experiment. The first two steps of Task B1 were intended to allow modeling teams to gain experience and develop modeling tools needed for simulating the more complex third step. The HE-E test is an *in-situ* experiment that is part of the performance of engineered barrier systems (PEBS) project, funded by the seventh framework project of the European Commission. The eight modelling teams involved in Task B1 are using different modeling tools (e.g., OpenGeoSys, EPCA3D, TOUGH-FLAC, COMSOL, FLAG, THAMES, and *xFlo*-FLAC).

The first step of Task B1 focuses on the THM processes in the HE-D test that was run in 2004–2005, including 340 days of heating. For this test, a heater was embedded in direct contact with the host rock, which is an indurated claystone called the Opalinus Clay. The main objectives of the HE-D experiment were to determine (i) thermal properties of the Opalinus Clay based on *in-situ* test results and (ii) effects of temperature on the hydromechanical behaviour of the Opalinus Clay (Wileveau and Rothfuchs, 2007; UPC, 2007). The test included measurements of temperature at 16 locations in the heated borehole and 23 locations in the rock mass. Pore water pressure was monitored using piezometers at 11 locations and rock strain was monitored using extensometers in 2 boreholes. THM processes in the Opalinus Clay host rock were evaluated based on the HE-D experiment and parameter estimates from the literature (Wileveau and Rothfuchs, 2007; UPC, 2007; Jobmann, et al., 2006). The results of the evaluation will help determine the appropriate THM properties for the HE-E test (Gaus, et al., 2014) host rock.

The HE-D test and related modeling work has been documented in several reports (e.g., Wileveau, 2007; UPC, 2007; Jobmann, et al., 2006) and journal papers (Gens, et al., 2007). Previous analysis of the HE-D test indicated that (i) the host rock can be considered

[1]http://decovalex.org/index.html

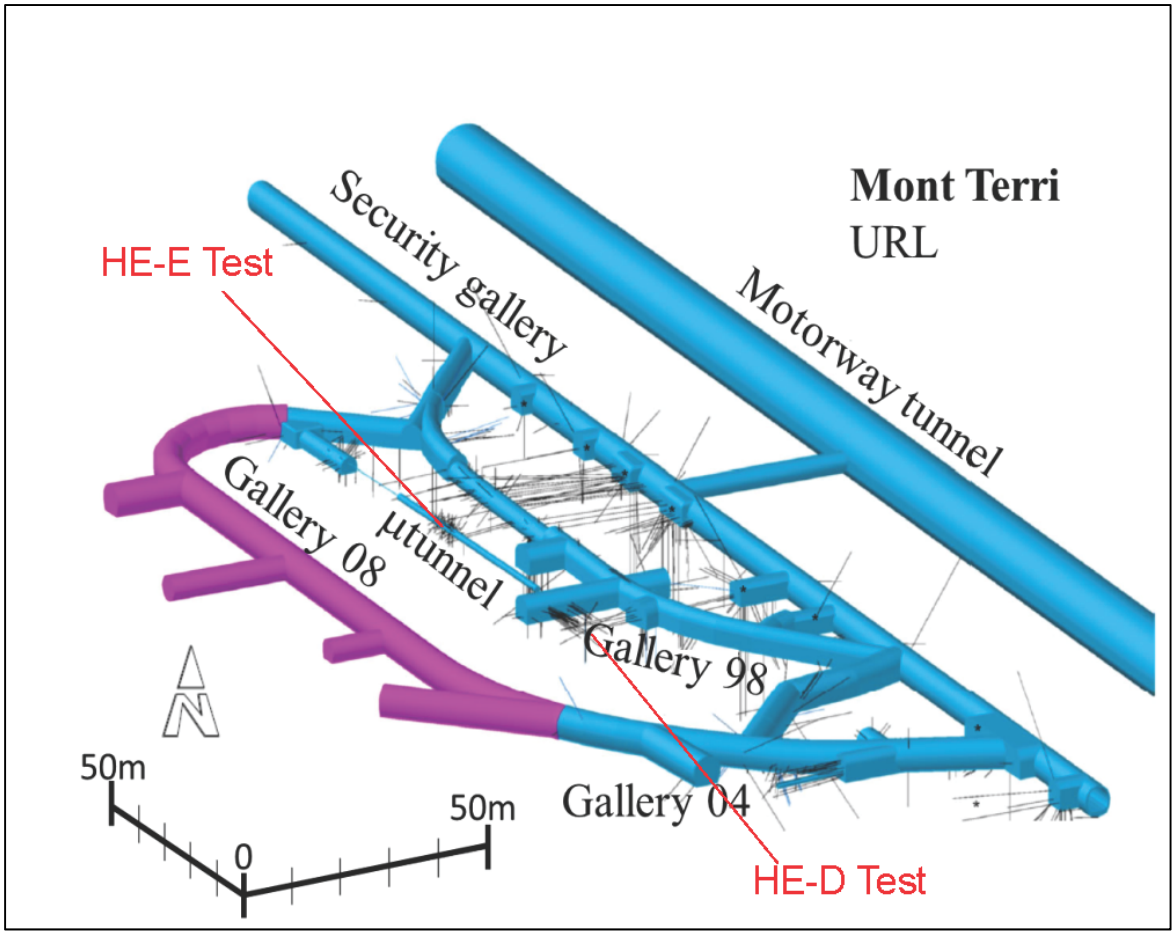

Figure 1-1. Locations of the HE-D and HE-E Tests at the Mont Terri URL, Switzerland (Modified From Garitte, et al., 2013)

linear-elastic and saturated under the conditions of the test and (ii) the important processes are heat conduction through the rock, thermal expansion of the rock and pore fluid, thermally induced pore pressure generation, time-dependent dissipation of excess pore pressure, and rock deformation caused by these processes. The FLAC code (Itasca Consulting Group, 2011) is adequate and well-suited to model these processes. Therefore, staff modeled the HE-D test using FLAC. The *xFlo*-FLAC code will be used for subsequent subtasks of Task B1.

1.1 Description of HE-D Test Setting

The HE-D experiment was set up as a mock-up test to support a similar experiment by ANDRA (Wileveau and Rothfuchs 2007; Zhang, et al., 2007). The Mont Terri URL was built as an extension of a security gallery of a highway tunnel in northwest Switzerland. The Mont Terri Project started in 1995 as an international collaborative effort to investigate hydrogeological, geochemical and geomechanical characteristics of the Opalinus Clay as a host rock for a geologic repository. The rock is a stiff overconsolidated clay consisting mainly of sheet silicates (illite, illite–smectite mixed layers, chlorites, kaolinites), framework silicates (albites, K-feldspar), carbonates (calcite, dolomite, ankerite and siderite), and quartz (Gens, et al., 2007). The bedding planes dip 30–50° toward the southwest (Wileveau, 2005). Jobmann, et al. (2006) described the heater and observation boreholes for the test, which were drilled from existing

underground openings into an area of the rock mass that can be considered homogenous with low fracture density and not intersected by any fault or shear zones. Also, the orientations of the existing underground openings permitted drilling observation boreholes parallel and perpendicular to the heater borehole.

The heater borehole was 14 m [46 ft] long with a diameter of 30 cm [12 in] (Gens, et al., 2007; Wileveau and Rothfuchs 2007). The heater assembly consisted of two heaters 0.8 m [2.6 ft] apart. Each heater is encased in a rubber membrane designed to transfer mechanical pressure and heat to the borehole wall. The pressure applied to the borehole wall was held at 0.1 MPa [14.5 psi] during the test. Monitoring sensors were installed in the 24 monitoring boreholes around the heater before the heater borehole was drilled and installed. Appendix A shows the layout of the heater borehole and some of the temperature and porewater pressure monitoring sensors. The heaters were switched on with a total power of 650 W (325 W per heater) 1 month after installation and pressurization and the heat load was maintained for 90 days. The power was then increased to 1,950 W (975 W per heater) for 248 days, after which the heaters were turned off. After 109 days, a leak caused depressurization of one of the heaters; however, this event did not appear to affect the test (Gens, et al., 2007). Monitoring continued for more than 7 months during the cooling phase.

1.2 Thermal-Hydrological-Mechanical Coupled Processes

A conceptualization of important THM processes for a saturated argillite subject to thermal loading conditions of the HE-D test is shown in Figure 1-2. Thick red solid lines indicate strongly coupled processes, thin black solid lines indicate moderately coupled processes, and dashed black lines indicate uncertain or weakly coupled processes.

The emplaced heat source causes temperatures to rise and thermal expansion of the pore water and rock matrix. Except for a small zone adjacent to the heaters, temperatures in the HE-D test remained below 100ºC [212ºF]. The zone where water could potentially have flashed to steam is small enough so as to likely have minimal impact on heat and moisture transfer elsewhere in the domain. Even in the small zone adjacent to the heaters, temperatures were expected to have remained well below that needed for alteration of the clay minerals. In addition, convection can be assumed negligible given the low permeability of the Opalinus Clay. Thus, conduction is the dominant mode of heat transfer. It is also assumed that other thermal processes are negligibly influenced by the hydrological-mechanical (HM) processes. With the level of the heat load imposed in the HE-D test along with the low permeability (nominally 5E-20 m^2) and porosity (0.137) of the Opalinus Clay, the host rock remains essentially saturated. This saturated condition implies that potential effects of the hydrological processes on the thermal parameters (mainly the thermal conductivity) are negligible. The small zone of unsaturated conditions that may occur near the heater, and the associated changes in thermal and hydrological properties, would be expected to have a negligible effect on temperature, stress, and hydrological conditions at nearly all measurement locations in the experiment. A change in porosity due to mechanical deformation could affect thermal conductivity, but, as discussed later, potential porosity changes are too small to have any appreciable effect. In general, anisotropy in thermal properties can be expected for argillites given their planar layers. Previous studies reported anisotropy in the bed-parallel and bed-normal thermal conductivities for the Opalinus Clay at the HE-D test (Gens, et al., 2007; Wileveau and Rothfuchs, 2007; UPC, 2007).

In a saturated argillite, the hydrologic processes result in changes in the pore pressure and are mainly dependent on the permeability and porosity of the host rock. The construction activities

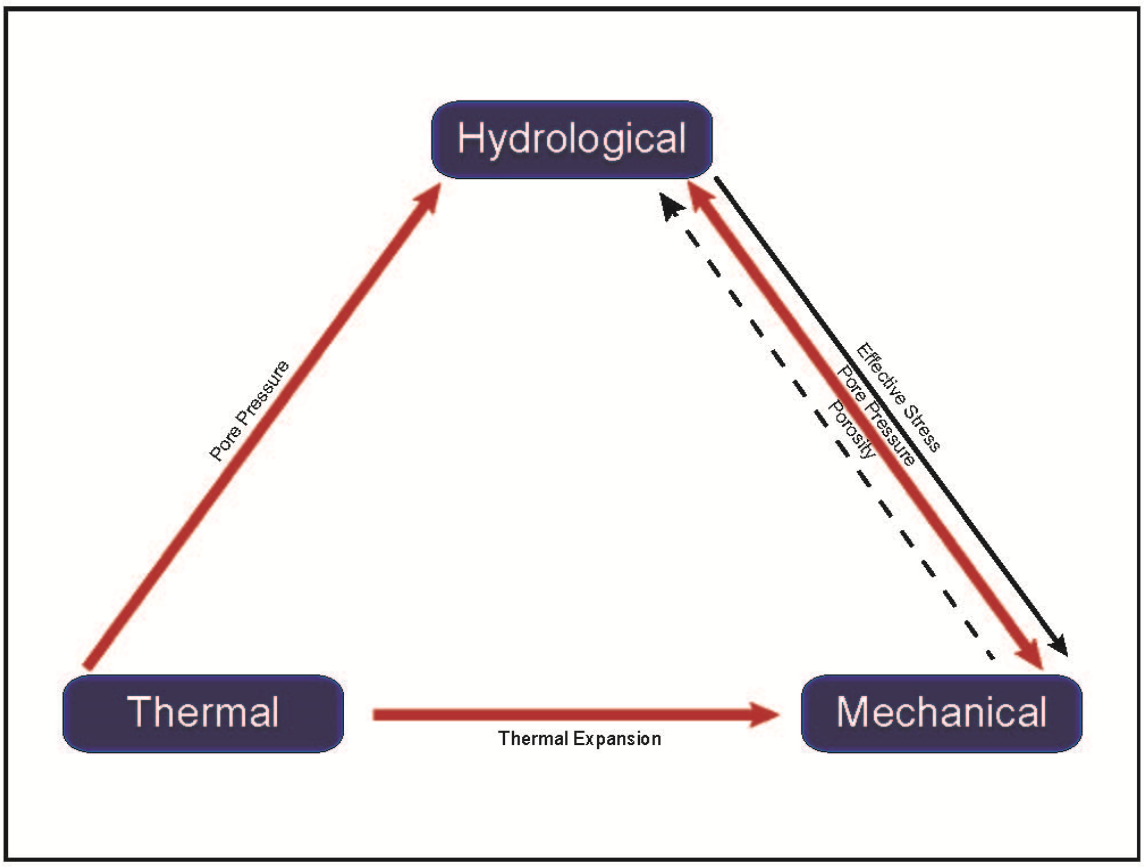

Figure 1-2. Conceptualization of Thermal-Hydrological-Mechanical Interactions for the HE-D Test

can influence the pore-pressure distribution. The effect of constructing the heater borehole on the HM conditions in the host rock was observed at the HE-D test (Wileveau and Rothfuchs, 2007). Some of the monitoring locations reported an increase in pore pressures as the drilling progressed. The spatial and temporal distribution of pore pressure during the heater test is determined by a balance of (i) the pore-pressure increase because of imposed thermal loads and (ii) pore-pressure dissipation dependent on permeability of the host rock and the pore pressure gradient. An increase in temperature causes an increase in pore pressure and the excess pore pressure dissipates as the heater shuts off. The pore pressure increase can be attributed to the differential expansion of water and rock matrix (i.e., for the same temperature interval, water expands more than the rock matrix). The permeability of the host rock controls the rate of pore pressure dissipation; low permeability values measured for Opalinus Clay imply that the dissipation rate is slow leading to a build-up of pore pressure. Local pore-pressure gradient at a location is influenced by its proximity to a boundary (drainage boundary) or heat source. The pore pressure changes will also influence changes in effective stress. The anisotropy in thermal-hydrological (TH) properties influences the evolution of the pore-pressure distribution.

The stress state in the host rock changes because of (i) activities such as excavation, (ii) emplacement of heaters (i.e., thermal expansion), and (iii) changes to pore water pressure.

Rock excavation consists of removing the static support the excavated rock previously provided. Potential thermal expansion in a rock matrix is partially suppressed because of nonuniform heating of the rock mass (e.g., rock temperature change varies spatially and temporally) and leads to thermal stress. In saturated argillites, suppressed thermal expansion of pore water results in an increase in pore-water pressure. These factors alter the stress state and the rock deforms to adjust to a new equilibrium state. The deformation in the rock could be elastic (fully reversible) or inelastic. Inelastic deformations may be expressed through formation of new cracks; slip, or opening or closing of existing cracks, or particle morphology changes not associated with cracking. Considering the rock strength [unconfined compressive strength of the Opalinus Clay is given as 10–16 MPa [1,450–2,321 psi] (Wileveau, 2005, Table 2-1)] and the range of rock stress anticipated during the HE-D test, the authors expect rock deformation to be mostly elastic. Any inelastic deformation, if it occurred, and resulting increase in porosity would be restricted to a narrow zone close to the borehole wall. Because the borehole wall is a drainage boundary {subjected to a controlled pore pressure of 0.1 MPa [14.5 psi] during the test}, a porosity increase near the borehole wall will have a negligible effect on pore pressure. Furthermore, porosity change due to elastic deformation will be negligible because the rock has a small initial porosity. Therefore, hydrologic processes are not expected to be significantly affected by porosity changes.

2 DESCRIPTION OF THE HE-D TEST NUMERICAL MODEL

Figure 2-1 shows the location of the HE-D test in the in the clay-rich shaly facies near the main gallery (Ga98) and the MI niche. A two-dimensional (2D), axisymmetric model centered on the axis of the heated borehole was setup for the THM modeling (Figure 2-2). An axisymmetric model is appropriate for a cylindrical source embedded in a semi-infinite, homogenous, and isotropic medium. The assumption of a semi-infinite medium is justified because the rock mass is orders of magnitude larger than the test dimensions. The assumption of homogeneity is justified because the fault zone and facies change (indicated in Figure 2-1) and the MI niche (Figures 2-1 and 2-2) are too far apart to influence the host rock response during the test. This assumption is justified for the thermal response because of the short duration of the test but may not be justified for the hydrological response. The assumption of isotropy is more difficult to justify because the host-rock thermal conductivity and permeability are likely different in bed-normal and bed-parallel directions. Potential implications of the bedding anisotropy are examined further in this report. The heater borehole radius for the HE-D test is 0.15 m [0.49 ft]. The model dimensions {8 × 28 m [26 × 92 ft]} and grid details are shown in Figure 2-3. The direction of the x-axis in Figure 2-3 corresponds to the radial direction (r) (i.e., in the direction of MI niche) in Figure 2-2. The direction of the y-axis in Figure 2-3 corresponds to the height (h) (i.e., away from the HE-D Niche) in Figure 2-2. Table B1 (Appendix B) lists the original and modified radial coordinates of the monitoring locations discussed in this report. A uniform grid spacing of 0.2 m [0.7 ft] was used along the y-axis. Along the x-axis, the grid spacing was increased from 0.05 to 0.895 m [0.16 to 2.94 ft] gradually outward from the heater borehole.

The exterior boundary of the model cylindrical rock body was placed at a distance of 8 m [26 ft] from the borehole axis. Thus, the exterior boundary corresponds approximately with the nearby MI niche. The effect of the open wall of the MI niche is not included in the model because the effect of the open wall of the niche was thought to be of secondary importance. Instead, thermal, pore pressure, and stress conditions consistent with the conditions at a radial distance of 8 m [26 ft] from the borehole axis are simulated at the exterior boundary. The simulated boundary conditions are assumed uniform over the surface of the modeled cylindrical rock body as is customary for an axisymmetric model.

Each analysis consisted of several phases representing (i) borehole excavation, (ii) placement of heating elements and tubing (after excavation), (iii) pressurization; (iv) first heating phase, (v) second heating phase, and (vi) cooling phase (UPC, 2007). Figure 2-3 shows the thermal and hydrological boundary conditions used for the model based on information from UPC (2007). Also, the geomechanical boundary conditions listed in Table 2-1 were based on the UPC model (UPC 2007, Table 4). The model simulation time is controlled by the heating time. The initial temperature is set to 15 °C [59 °F] everywhere. The initial pore pressure distribution was obtained from a steady-state simulation based on the hydrological boundary conditions (Figure 2-3) without any sources or sink.

The modeling relied on a few assumptions that were made to simplify the modeling effort to a level commensurate with the objectives. First, the host rock within the model domain was assumed to be saturated. Although, unsaturated conditions may have occurred near the heater, MI niche, HE-D Niche, and New Gallery, the affected volume was assumed insignificant. The assumption of saturated conditions, based on previous studies (Wileveau and Rothfuchs, 2007; UPC, 2007), is common to all the DECOVALEX modeling teams, and is justified by positive pore-water pressure response at the monitored boreholes. Second, it was assumed that heat flow and temperature change affect but are not affected by the hydrological and mechanical

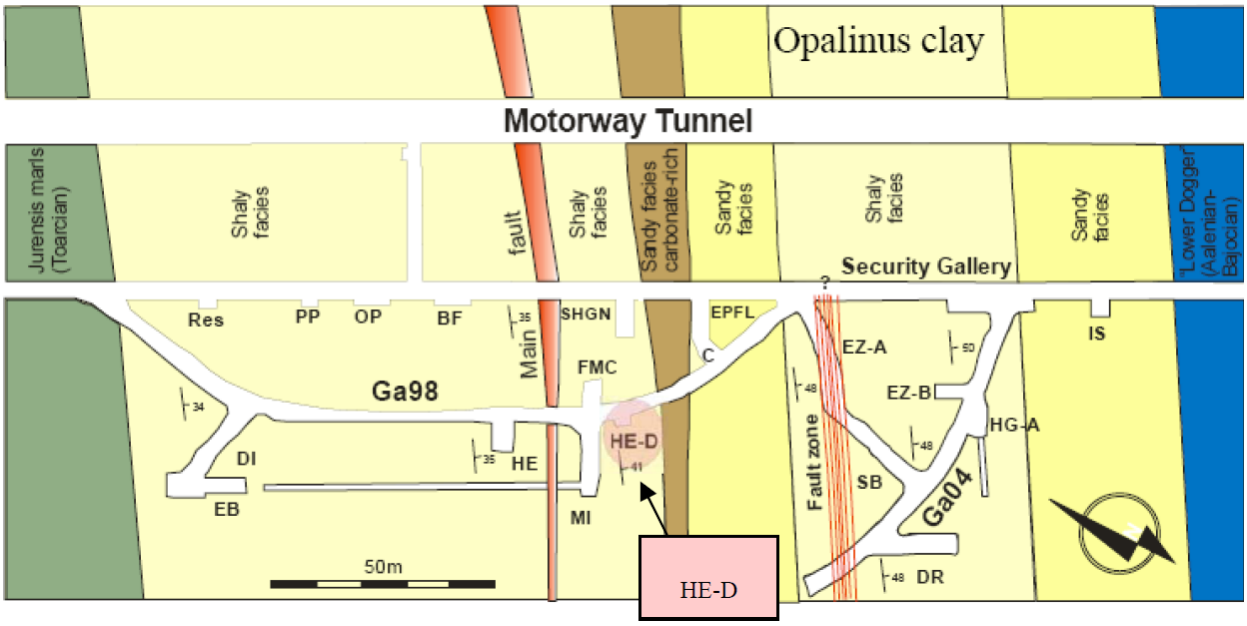

Figure 2-1. Horizontal Cross Section of the Mont Terri Rock URL Showing the Location of the HE-D Test Field (Wileveau and Rothfuchs, 2007)

processes. This assumption is valid for a saturated rock, and mechanical conditions (e.g., those discussed in Section 1.2) are unlikely to result in a significantly changed porosity. The assumption implies that the thermal conductivity of the host rock is not influenced by HM processes. Third, it was assumed that the existing underground openings have no significant effect on thermal, hydrological, and mechanical conditions at the monitored locations. Borehole excavation and its effects on HM conditions are included in the model but the HE-D and MI niche openings are not included. Based on observations at measurement locations and on analysis of modeling results, the effect of the openings appears to be secondary and was considered in a qualitative manner when evaluating simulation results. Finally, it was assumed that details of the heater components have no effect on THM processes in the host rock. Therefore, the model includes the heater as a heat source and pressure boundary but does not include details of the heater components.

The analysis focused on determining the evolution of temperature (T) and pore water pressure (u_w) in response to the heat load. Temperature should increase or remain essentially unchanged everywhere within the model domain. The pore pressure evolution depends on the heat load, bulk thermal properties, mechanical properties of liquid water, and the rock-mass permeability. The heat load should cause the pore pressure to increase but the excess pore pressure should dissipate at a rate that depends on the prevailing hydraulic conductivity and distance to the drainage boundary. The rock-mass thermal conductivity and permeability could be affected by the rock-mass stratigraphy and structure; particularly, the bedding. The effects of these rock-mass and water properties on the THM response will be explored through the numerical modeling. The applied heat loads are shown in Figure 2-4. Also, Figure 2-5 shows the locations monitored for temperature, pore-water pressure, and rock strain in the 2D axisymmetric model. The locations, monitored for both temperature and pore pressure, are also shown in Figure 2-6 in terms of the bed-normal and bed-parallel components of the distance to the heater. Table B–1 (Appendix B) also provides the numerical values for the bed-normal and bed-parallel components at these locations.

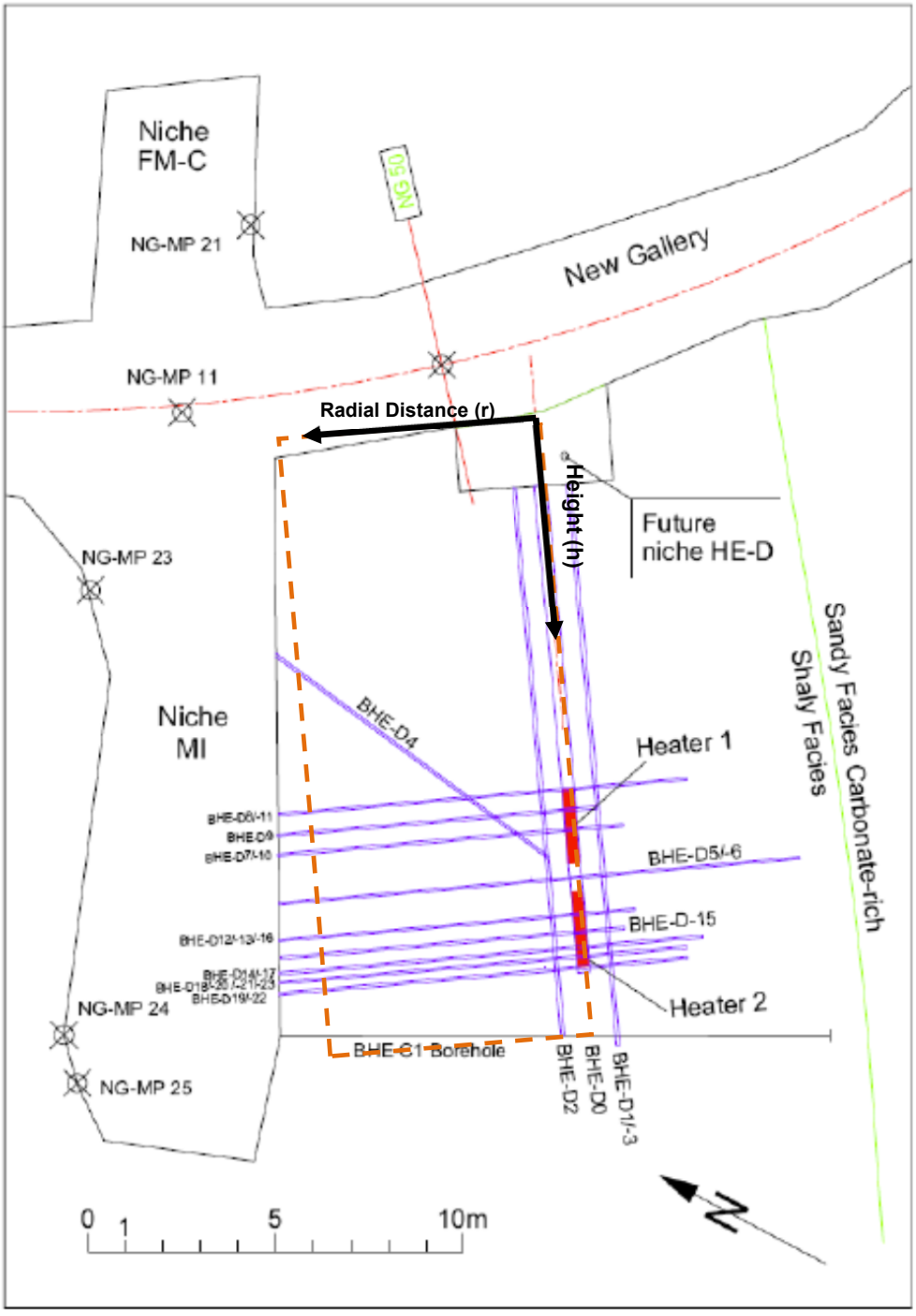

Figure 2-2. Layout of the HE-D Experiment (Wileveau and Rothfuchs, 2007; UPC, 2007) and the Outline of an Axisymmetric Numerical Model (Dashed Rectangular Box) [1 m = 3.28 ft]

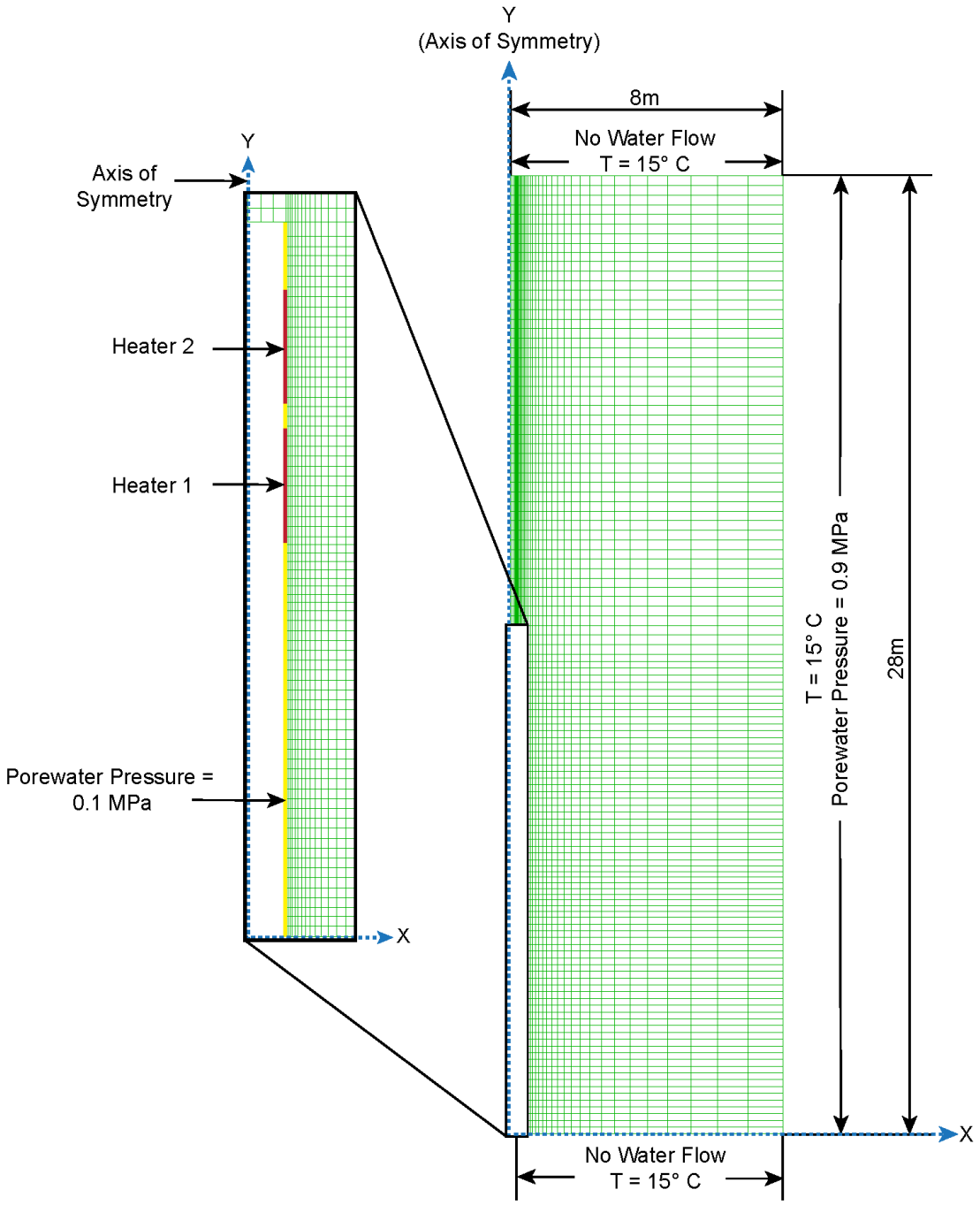

Figure 2-3. Axisymmetric Model Mesh and Thermal-Hydrological Boundary Conditions. Yellow Line Represents the Pore-Water Pressure Applied to the Inner Wall of the Heater Borehole. The Borehole is 14 m Long and 0.3 m in Diameter. Each Heater is 2 m Long. [1 m = 3.28 ft; °F = (1.8 × T °C + 32)]

Table 2-1. Mechanical Boundary Conditions				
Boundary		**Excavation Stage**	**Heater Placement**	**Pressurization, Heating Phases 1 and 2, and Cooling Stages**
A	X = 0 to 8 m Y = 0	σ_n = 4.28 MPa	σ_n = 4.28 MPa	σ_n = 4.28 MPa
B	X = 8 m Y = 0 to 28 m	σ_n = 4.28 MPa	σ_n = 4.28 MPa	σ_n = 4.28 MPa
C	X = 0 to 8 m Y = 28 m	y-disp = 0	y-disp = 0	y-disp = 0
D	X = 0 Y = 14 to 28 m	x-disp = 0	x-disp = 0	x-disp = 0
E	X = 0.15 m Y = 12.775–14 m	Borehole Excavated in steps	σ_n = 0.1 MPa	σ_n = 0.1 MPa
F	X = 0.15 m Y = 10.775–12.775 m Heater		σ_n = 0.1 MPa	σ_n = 1.1 MPa
G	X = 0.15 m Y = 10–10.775 m		σ_n = 0.1 MPa	σ_n = 0.1 MPa
H	X=0.15, y=8–10 m Heater		σ_n = 0.1 MPa	σ_n = 1.1 MPa
I	X = 0.15 m Y = 6.5–8 m		σ_n = 0.1 MPa	σ_n = 0.1 MPa
J	X = 0.15 m Y = 0–6.5 m		x-disp = 0	x-disp = 0
1 m = 3.28 ft 1MPa = 145 psi				

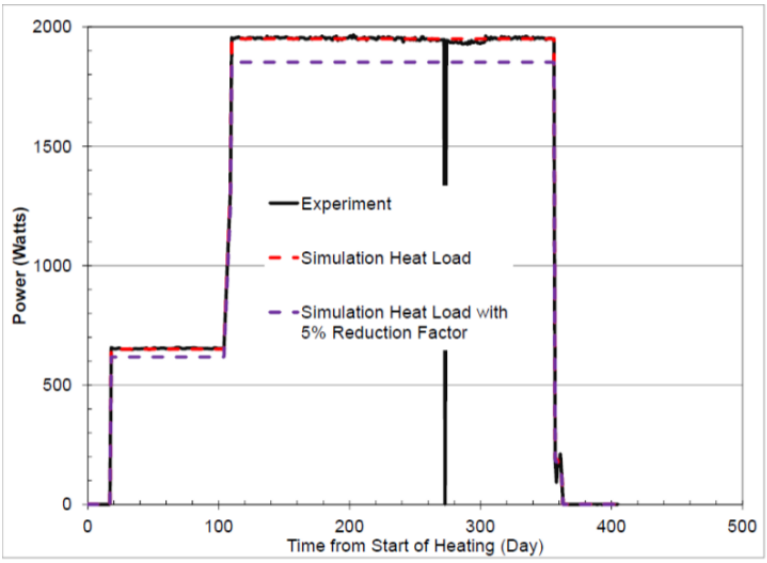

Figure 2-4. Thermal Load History Applied in the Experiment and Numerical Model (From Garitte, et al., 2007, Figure 10). The Thermal Load Was Reduced by 5 Percent in One of the Analysis Cases Described in Section 2.3.

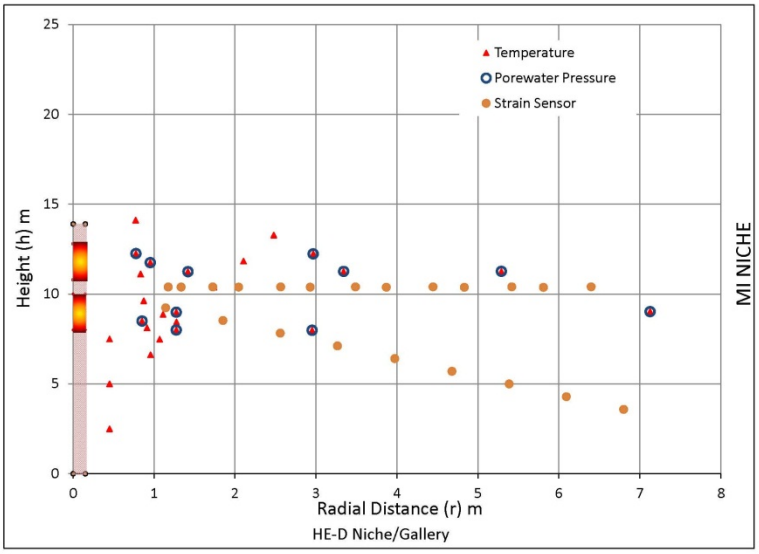

Figure 2-5. Locations Monitored for Temperature, Pore-Water Pressure, and Rock Strain, Shown in Model Cylindrical Coordinates [1 m = 3.28 ft]

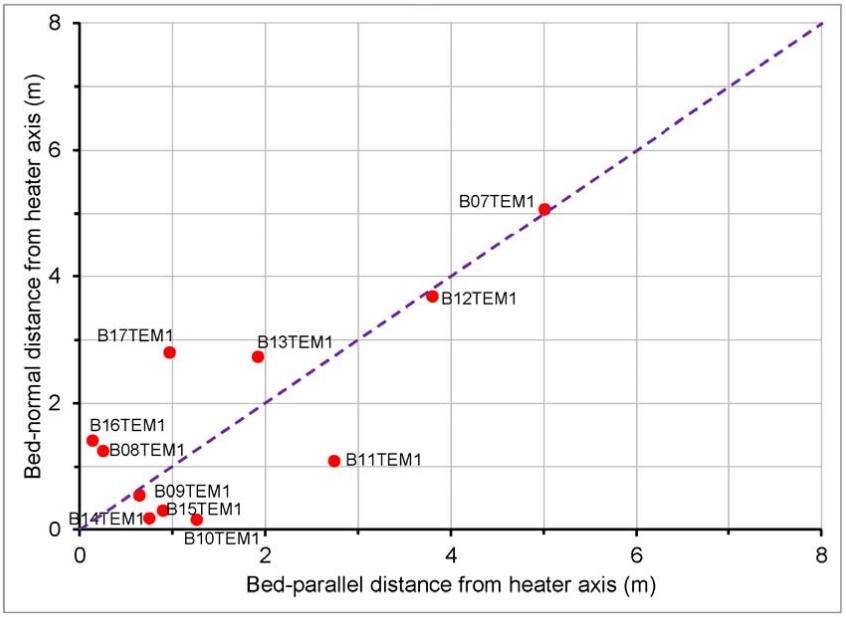

Figure 2-6. Locations Monitored for Both Temperature and Pressure, Shown With Reference to a Cartesian Coordinate System Based on the Bed-Normal and Bed-Parallel Distance From Heater [1 m = 3.28 ft]

2.1 Modeling Approach Using FLAC Computer Code

The processes are modeled in FLAC (Itasca Consulting Group, 2011) through sequentially coupled thermal (heat conduction), hydrological (flow of water driven by combined temperature and pore pressure gradients), and mechanical (deformation and rock stress evolution due to changing temperature and pore pressure) analyses. Thermal analysis through heat conduction alone is justified for the HE-D test because the host rock has very low permeability, such that heat transfer from water flow is negligible compared to conduction. The hydrological analysis includes (i) using the thermal expansivity of water and soil skeleton and bulk modulus of water to evaluate pore pressure changes due to temperature changes and (ii) using Darcy's law to evaluate water flow and pore pressure dissipation. The mechanical analysis uses linear elasticity to evaluate deformations of the solids skeleton and changes in effective stress. The stresses developed are not great enough to cause plastic yielding, so the mechanical constitutive model was limited to linear elasticity. The THM calculations begin with thermal analysis to evaluate temperature changes in the host rock. Then thermal volumetric strains are introduced into the mechanical and fluid constitutive laws to account for thermally induced stress and thermal-pore pressure couplings (Itasca Consulting Group, 2011). The thermal-fluid coupling evaluates the change in pore pressure resulting from the thermal expansion of the fluid and solid constituents. In coupled fluid-mechanical simulation, the pore pressure increment changes effective stress and affects the mechanical response of the material. Additionally, mechanical volume changes cause changes in pore pressure. The three-way coupled analyses cannot be directly conducted in FLAC; thus, a user-defined structure was developed coupling thermal, mechanical, and flow analyses using FISH, a programming language within FLAC.

The thermal properties for heat transfer analysis are thermal conductivity and specific heat. The mechanical properties are bulk and shear moduli, which are determined from the Young's modulus (E) and Poisson's ratio (υ). The thermal-coupling parameter for thermal-mechanical analysis is the volumetric thermal expansivity (β_g) of the solid particles. Parameter values used for the analyses are given in Tables 2-2 and 2-3.

Water flow modeling is based on Darcy's law. The properties needed for water flow analysis are the intrinsic permeability (κ) of the rock and dynamic viscosity of water (μ_w). FLAC uses the ratio κ/μ, referred to as the fluid mobility coefficient. Fluid flow coupling to the thermal calculation is provided through the volumetric thermal expansivities of the water (β_w) and solid particles. Fluid-mechanical coupling in FLAC is based on Biot's theory. In the HE-D analysis, the compressibility of solid particles is considered negligible relative to the compressibility of the solids skeleton (drained compressibility of the clay shale), which implies a Biot coefficient equal to unity (i.e., $\alpha = 1$). Therefore, the properties needed in the model for coupled fluid-deformation analysis are fluid bulk modulus (K_w) and rock porosity (n). The Biot modulus (M), which is not a direct input to the model, is equal to the ratio of K_w/n (Itasca Consulting Group, 2011).

The parameters for water properties—namely, density (ρ_w), thermal expansivity (β_w), bulk modulus (K_w), and viscosity (μ_w)—are functions of temperature and pressure (temperature only for viscosity) as described in Section 2.2. Thus, the mobility coefficient is also a function of temperature. Because the rock temperature changes as the thermal energy from the heater propagates into the rock medium (e.g., see temperature contours described in Chapter 3), the water parameters are computed for each grid point during every time increment in the thermal calculation. The calculation was incorporated in the FLAC models through FISH functions.

The overall calculation of flow using FLAC consists of the following. First, the model without the heater borehole was initialized to mechanical equilibrium with prescribed boundary stresses on

Table 2-2. Analysis Cases With Constant Properties for Liquid Water

Case Designator		D15 Case	D15 Case with Full Heat Load	CNWRA Basecase	CNWRA Case with Greater k
Heat Load		95%	100%	100%	100%
Heat flow parameters					
Bulk thermal conductivity, k_{th}	W/(m K)	1.77	1.77	2.40	2.40
Bulk Specific Heat Capacity	J/kg-K	1000	840	840	840
Density/Unit weight					
Water density, ρ_w	kg/m^3	Function of temp & pressure	Function of temp & pressure	Function of temp & pressure	Function of temp & pressure
Gravity, g	m/s^2	9.81	9.81	9.81	9.81
Porosity, n	(-)	0.137	0.137	0.137	0.137
Dry density ρ_d	kg/m^3	2313	2313	2313	2313
Permeability					
Intrinsic Permeability, κ	m^2	5.0E-20	5.0E-20	5.0E-20	5.0E-19
Dynamic Viscosity, μ	Pa-sec	Function of temp	Function of temp	Function of temp	Function of temp
Mobility coefficient, $k_{gw} = \kappa/\mu$	m^2/(Pa.s)	Function of dynamic viscosity & Intrinsic permeability	Function of dynamic viscosity & Intrinsic permeability	Function of dynamic viscosity & Intrinsic permeability	Function of dynamic viscosity & Intrinsic permeability
Elastic Stiffness					
Water bulk modulus, K_w	Pa	Function of water density	Function of water density	Function of water density	Function of water density
Rock Young's modulus, E	Pa	7.00E+09	7.00E+09	7.00E+09	7.00E+09
Poisson's ratio, ν	(-)	0.27	0.27	0.27	0.27
Rock bulk modulus = $E/3(1-2\nu)$	Pa	5.07E+09	5.07E+09	5.07E+09	5.07E+09
Rock shear modulus = $E/2(1+\nu)$	Pa	2.76E+09	2.76E+09	2.76E+09	2.76E+09
Biot modulus, $M = K_w/n$	Pa				
Volumetric Thermal Expansion					
Water thermal expansivity, β_w	(°C)$^{-1}$	Function of water density	Function of water density	Function of water density	Function of water density
Solid particle thermal expansivity, β_g	(°C)$^{-1}$	2.00E-05	2.00E-05	2.00E-05	2.00E-05

P = pressure, T = temperature, THM = coupled thermal-hydrological-mechanical analysis
"T Only" = "thermal-only analysis"

the right and bottom boundaries and zero normal displacement on the top and left boundaries (Figure 2-3). This analysis was accomplished using the explicit method where the model is iterated until a balanced state is reached. Second, the heater borehole is introduced in stages by removing elements and applying the pressure and zero displacement boundary conditions in appropriate segments as described in Table 2-1. The model was brought to static equilibrium to conclude each "excavation" stage. Third, the initial temperature and pore pressure distributions were established using the thermal and fluid boundary conditions shown in Figure 2-3. The initial temperature was set to 15 °C [59 °F] everywhere and the initial pore pressure distribution was calculated through fluid flow analysis. Fourth, the heat flux was applied at the heater locations (Figure 2-3) as described in Figure 2-4. FLAC uses either explicit or implicit solution schemes for thermal and fluid flow analyses. The implicit solution scheme was found to be faster and was used for the thermal and fluid analyses during this phase. The thermal, hydrological, and mechanical analyses during this phase were coupled sequentially as follows: a thermal analysis step was performed to increment the thermal time from t to $t + \Delta t$; thereafter, mechanical analysis was performed to establish equilibrium at time $t + \Delta t$; then as many fluid-flow steps as necessary are performed to advance the hydrological state from time t to

Table 2-3. Analysis Cases With Temperature- and Pressure-Dependent Liquid Water Properties

Case Designator		D15 Case	D15 Case with Full Heat Load	CNWRA Basecase	CNWRA Case with Greater k
Heat Load		95%	100%	100%	100%
Heat flow parameters					
Bulk thermal conductivity, k_{th}	W/(m.K)	1.77	1.77	2.40	2.40
Bulk Specific Heat Capacity	J/kg-K	1000	840	840	840
Density/Unit weight					
Water density, ρ_w	kg/m^3	Function of temp & pressure	Function of temp & pressure	Function of temp & pressure	Function of temp & pressure
Gravity, g	m/s^2	9.81	9.81	9.81	9.81
Porosity, n	(-)	0.137	0.137	0.137	0.137
Dry density, ρ_d	kg/m^3	2313	2313	2313	2313
Permeability					
Intrinsic Permeability, κ	m^2	5.0E-20	5.0E-20	5.0E-20	5.0E-19
Dynamic Viscosity, μ	Pa-sec	Function of temp	Function of temp	Function of temp	Function of temp
Mobility coefficient, $k_{gw} = \kappa/\mu$	$m^2/(Pa.s)$	Function of dynamic viscosity & Intrinsic permeability	Function of dynamic viscosity & Intrinsic permeability	Function of dynamic viscosity & Intrinsic permeability	Function of dynamic viscosity & Intrinsic permeability
Elastic Stiffness					
Water bulk modulus, K_w	Pa	Function of water density	Function of water density	Function of water density	Function of water density
Rock Young's modulus, E	Pa	7.00E+09	7.00E+09	7.00E+09	7.00E+09
Poisson's ratio, ν	(-)	0.27	0.27	0.27	0.27
Rock bulk modulus = $E/3(1-2\nu)$	Pa	5.07E+09	5.07E+09	5.07E+09	5.07E+09
Rock shear modulus = $E/2(1+\nu)$	Pa	2.76E+09	2.76E+09	2.76E+09	2.76E+09
Biot modulus, $M = K_w/n$	Pa				
Volumetric Thermal Expansion					
Water thermal expansivity, β_w	$(°C)^{-1}$	Function of water density	Function of water density	Function of water density	Function of water density
Solid particle thermal expansivity, β_g	$(°C)^{-1}$	2.00E-05	2.00E-05	2.00E-05	2.00E-05

$t + \Delta t$, with mechanical analysis performed to reestablish mechanical equilibrium after each fluid-flow step. The last set of mechanical analyses was necessary to ensure that each mechanical equilibrium state includes the current temperature and pore-pressure distributions.

The sequence of analyses at each time step were implemented through a FISH function. The thermal and fluid modules must be run independently in FLAC. The groundwater (i.e., hydrological) analysis module was suppressed to run a thermal calculation. Also, the thermal module was suppressed during a groundwater module calculation. However, the thermal and groundwater modules are coupled by using temperature distributions calculated in the thermal module as input for the groundwater module. In addition, the mechanical response is coupled to the thermal and hydrological responses by running enough mechanical analysis cycles to obtain a mechanical equilibrium state that includes the current temperature and pore pressure distributions. The FISH function controls the calculations with sequential coupling as described while stepping through the thermal load history in Figure 2-4. The calculated temperature, pore pressure, and stresses and displacements are stored at each thermal time (t, $t + \Delta t$, etc) at selected locations, such as the monitored locations for the HE-D test (e.g., Figures 2-2 and 2-5).

2.2 Liquid Water Properties as Functions of Temperature and Pressure

Data from National Institute of Standards and Technology (NIST) Steam Table (NIST, 2011) for the temperature range of 10–98 °C [50–208 °F] and pressure range of 0.1–10 MPa [14.5–1,450 psi] were used to develop relationships for liquid water mechanical properties: density (ρ_w), thermal expansivity (β_w), bulk modulus (K_w), and viscosity (μ_w) as functions of temperature and pressure. The following relationships were obtained. The relationships are shown graphically in Figures 2-7 and 2-8.

$$\rho_w = \rho_{10} + c_1(T-10) + c_2(T-10)^2 + c_3(T-10)^3 \qquad (10 \le T \le 100\ ℃) \qquad (2\text{-}1)$$

$$\rho_{10} = b_0 + b_1 P \qquad (0 \le P \le 10\ \text{MPa}) \qquad (2\text{-}2)$$

where

$b_0 = 999.7525$
$b_1 = 0.4747475$
$c_1 = -0.11487$
$c_2 = -4.9696 \times 10^{-3}$
$c_3 = 1.2671 \times 10^{-5}$

$$\beta_w = -\frac{1}{\rho_w}\frac{\partial \rho_w}{\partial T} \qquad (2\text{-}3)$$

$$\frac{\partial \rho_w}{\partial T} = c_1 + 2c_2(T-10) + 3c_3(T-10)^2 \qquad (10 \le T \le 100\ ℃)$$

The parameters c_1, c_2, and c_3 are functions of pressure but their relationship with pressure is not evaluated using Eq. (2-1). Instead, the dependence of ρ_w on pressure is approximated using Eqs. (2-1) and (2-2) with c_1, c_2, and c_3 treated as constants; whereas $\frac{\partial \rho_w}{\partial P}$ is evaluated by fitting ρ_w versus P data at various temperatures as described in the following

$$K_w = 1/b_w \qquad (\text{MPa}) \qquad (2\text{-}4)$$

$$b_w = \frac{1}{\rho_w}\frac{\partial \rho_w}{\partial P} \qquad (2\text{-}5)$$

$$\frac{\partial \rho_w}{\partial P} = f_{10} + a_1(T-10) + a_2(T-10)^2 + a_3(T-10)^3 \quad (10 \le T \le 100\ ℃) \quad (0 \le P \le 10\ \text{MPa}) \qquad (2\text{-}6)$$

where

$f_{10} = 0.4747475$
$a_1 = -2.331 \times 10^{-3}$
$a_2 = 3.621 \times 10^{-5}$
$a_3 = -1.317 \times 10^{-7}$

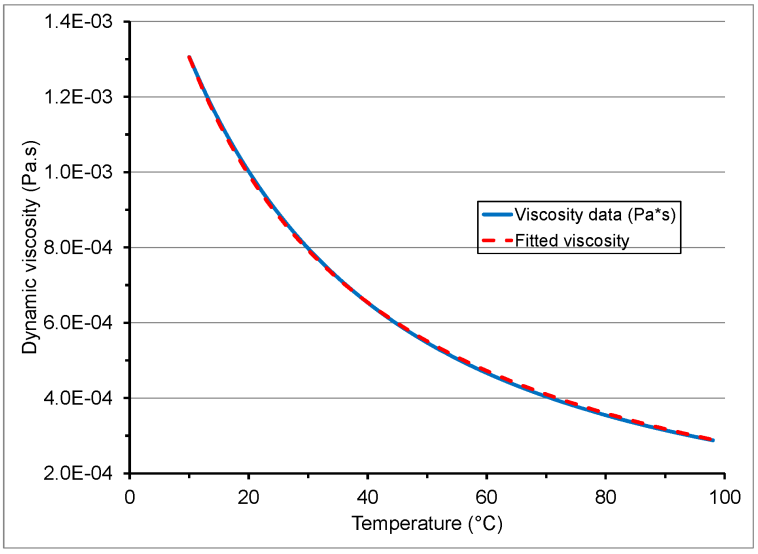

Figure 2-7. Dynamic Viscosity of Liquid Water as a Function of Temperature [°F = (1.8 × T °C + 32)]

$$\mu_w = \mu_{10} - \frac{T - 10}{d_1 + d_2(T - 10)} \qquad \text{(Pa.s)} \qquad (2\text{-}7)$$

$$(10 \leq T \leq 100\ ^\circ\text{C})$$

where

$\mu_{10} = 1.3055 \times 10^{-3}$
$d_1 = 2.50 \times 10^4$
$d_2 = 700$

where ρ_w, β_w, K_w, and μ_w are the water density (kg/m^3), thermal expansivity (volumetric strain per °C), bulk modulus (MPa), and viscosity (Pa.s), respectively.

2.3 Analysis Cases

Two sets of analysis were performed as described in Tables 2-2 and 2-3. The first set consists of calculation cases with liquid water properties assigned constant values (Table 2-2). For these cases, the bulk thermal conductivity (k_{th}) was varied as described in Table 2-2. Two cases with k_{th} = 2.4 W/(m.K) were analyzed to explore the effects of water bulk modulus and thermal expansivity on the calculated pore pressure (Basecase 1: K_w = 2.15 GPa and β_w = 5×10^{-4}/°C; and Basecase 2: K_w = 2.0 GPa and β_w = 3.5×10^{-4}/°C).

The second analysis set (Table 2-3) consists of cases with liquid-water properties varied with temperature and pressure as described in Section 2.2. One case (D15 Case) used thermal parameter values the DECOVALEX Task Lead for Task B1 recommended to provide a common set of parameters for all modeling groups. As shown in Table 2-3, a variation of this

case with full heat load and a bulk specific heat capacity of 840 J/kg.K (D15 Case with Full Heat Load) was analyzed to compare with the CNWRA basecase.

Also, a variation of the CNWRA basecase with the intrinsic permeability increased one order of magnitude (CNWRA Case with Greater k) was analyzed to explore the effects of permeability on calculated pore-water pressure.

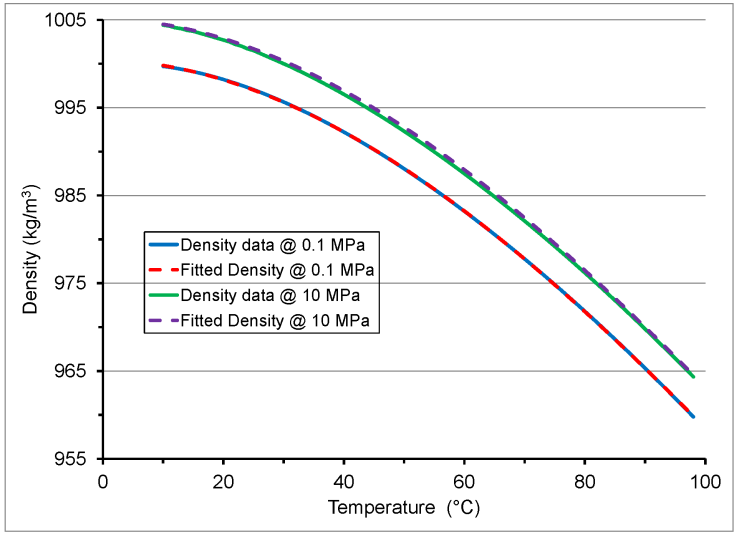

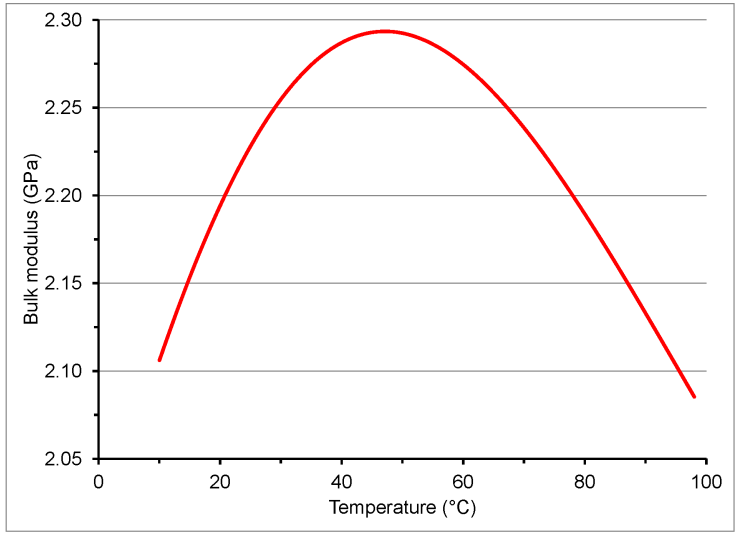

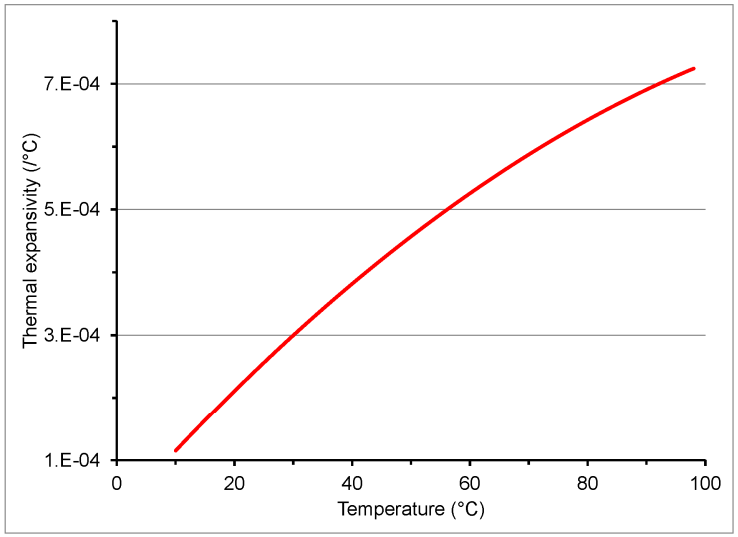

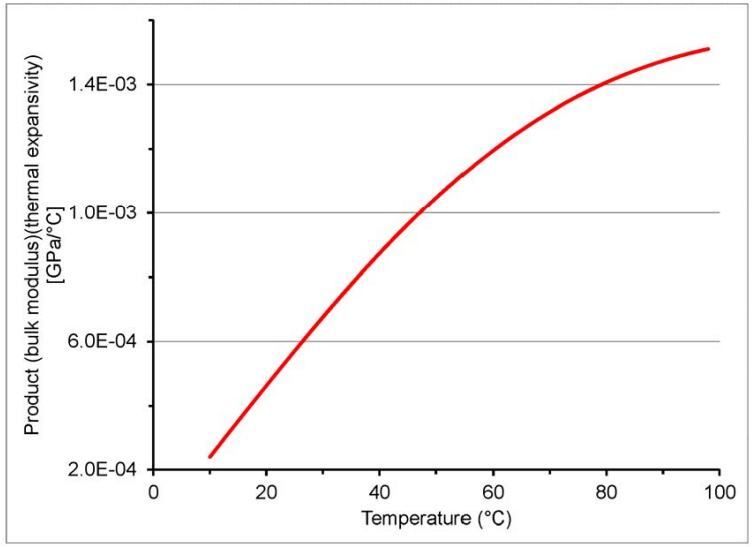

Figure 2-8. Liquid Water Density and Related Properties as Functions of Temperature and Pressure [°F = (1.8 × T °C + 32); 1 MPa = 145 psi]

3 CALCULATED RESPONSE

The calculated response is examined in this chapter through the sensitivity of temperature and pore pressure to various THM parameters. The results are examined to explore for possible effects of bedding anisotropy on the THM response of the rock mass. The purpose of the sensitivity analyses at the HE-D test location is to facilitate a better understanding of the effects caused by changes to parameters, rather than to estimate a best set of parameters from the HE-D test to apply to the HE-E test domain. Besides slight differences in the host rock at the two test locations, potential future improvements in the modeling capabilities may become available when the HE-E test is simulated.

3.1 Temperature Histories

Qualitative matching of temperature profiles at different locations in the HE-D test domain was used to estimate (i) an effective thermal conductivity for the entire domain that could be used in later calculations of pore pressure, displacement, and strain in this report; and (ii) the magnitude of anisotropic thermal conductivity. For the latter, an anistropic conceptual model is used that assumes different values of thermal conductivity for two directions relative to the bedding plane of the host rock, bed-normal and bed-parallel. Due to a constraint in FLAC, however, calculations are made using an isotropic implementation in the numerical model; FLAC uses a single value for an effective thermal conductivity. Different values of thermal conductivity are used in FLAC calculations to assess which one leads to the best matches of measured temperature profiles at locations depicted as bed-normal or bed-parallel relative to the heater. The purpose of analyzing implications of anistropic and isotropic thermal conductivity is to support future HE-E modeling decisions in final step of Task B1. In addition, comparisons with results from other Task B1 modeling teams, several of which have implemented anistropic models, can be used by staff to support future HE-E test modeling decisions.

The calculated temperature histories are compared with the measured temperature in Figures 3-1 through 3-3. In the figures, the monitored temperature locations are grouped in terms of the bed-normal and bed-parallel components of distance to the heated borehole, as graphed in Figure 2-6. The authors hypothesize that the effective thermal conductivity governing heat transfer from the heater to a monitored location is influenced more by the bed-normal conductivity for locations with a bed-normal distance component greater than the bed-parallel component (i.e., monitored locations above the broken line in Figure 2-6). For monitored locations below the broken line (i.e., locations for which the bed-parallel distance component is greater than the bed-normal component), the authors hypothesize that the effective conductivity is influenced more by the bed-parallel thermal conductivity. Although the geometric model used for the analyses restricts the simulated thermal conductivity to be isotropic, the effect of transverse isotropy in the rock mass thermal conductivity (i.e., different thermal conductivity in the bed-normal and bed-parallel directions but with all bed-parallel directions being equivalent) could be discerned from the relationships among the calculated and measured temperature histories if the previously noted hypotheses are correct. Figure 3-1 shows temperature histories at monitored locations above the broken line in Figure 2-6 (i.e., locations with a greater bed-normal than bed-parallel distance to the heater). As Figure 3-1 shows, the measured temperature histories at these locations are matched better using models with smaller thermal conductivity. The results shown in the figure suggest use of an effective (isotropic) thermal conductivity smaller than 1.77 W/m.K for modeling heat flow best represents heat flow in this area of the rock mass.

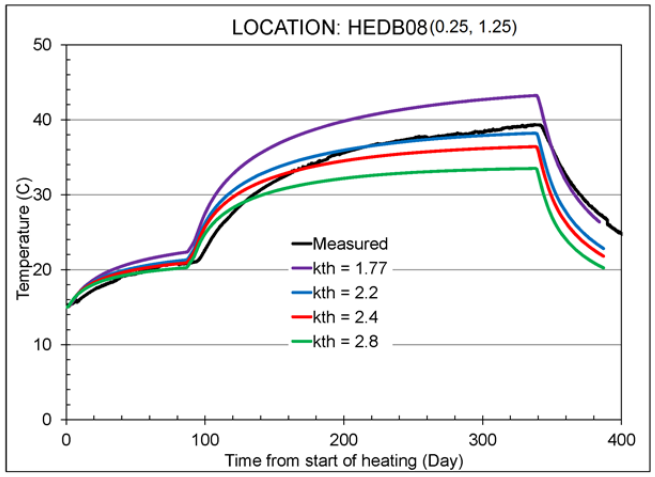

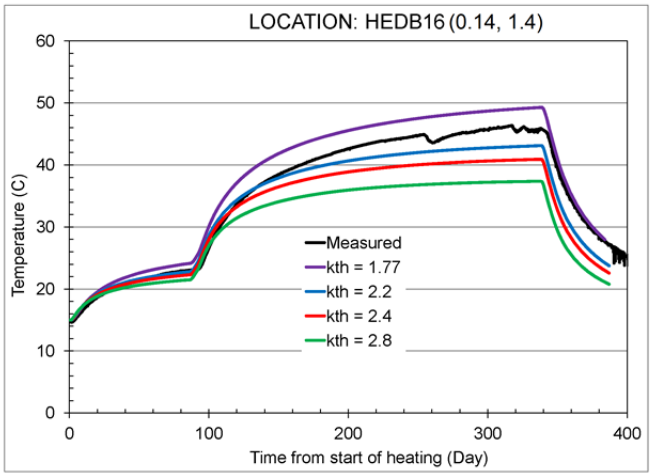

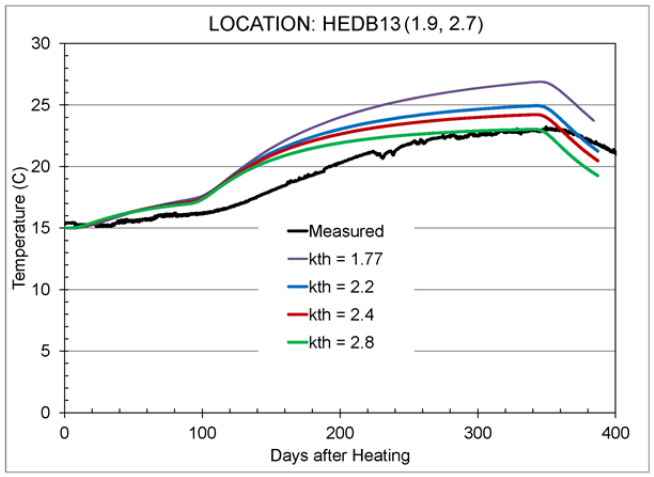

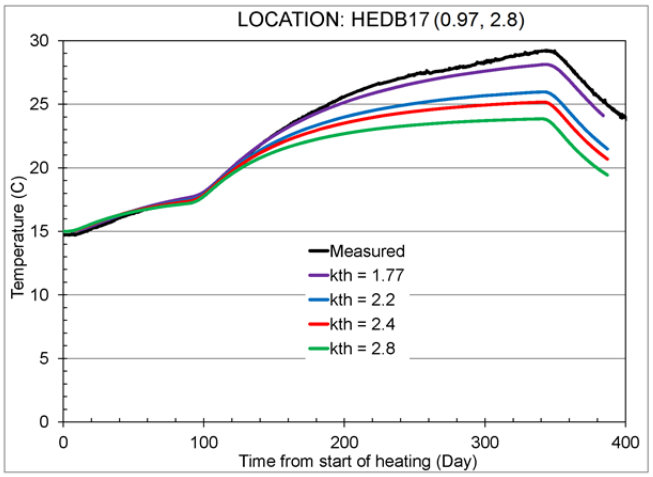

B13

Figure 3-1. Temperature Histories at Locations With Greater Bed-Normal Than Bed-Parallel Distance From the Heater Borehole, Showing the Effects of Thermal Conductivity (k_{th}). Coordinates in Parenthesis are the Bed-Parallel and Bed-Normal Distances (m) Shown in Figure 2-6. [°F = (1.8 × T °C + 32), 1 m = 3.28 ft]

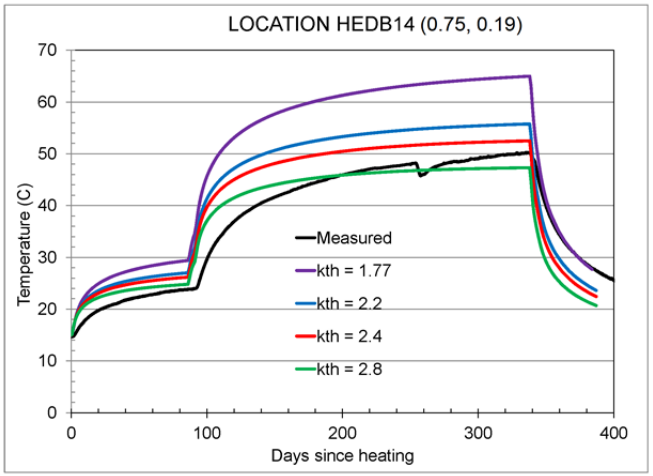

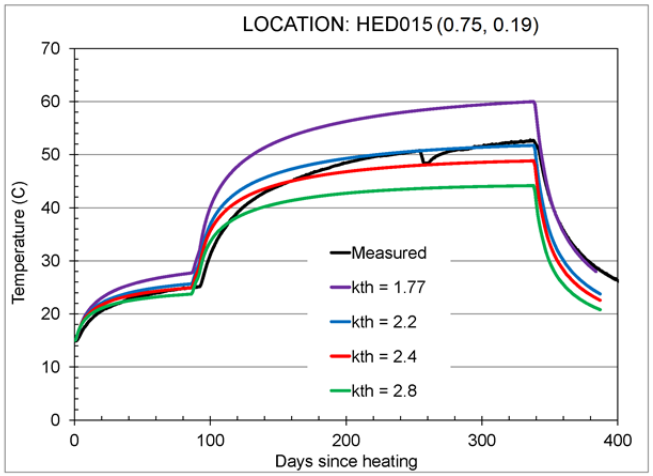

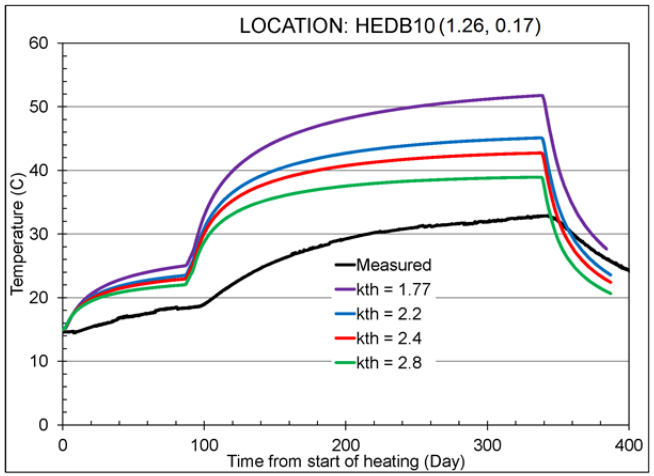

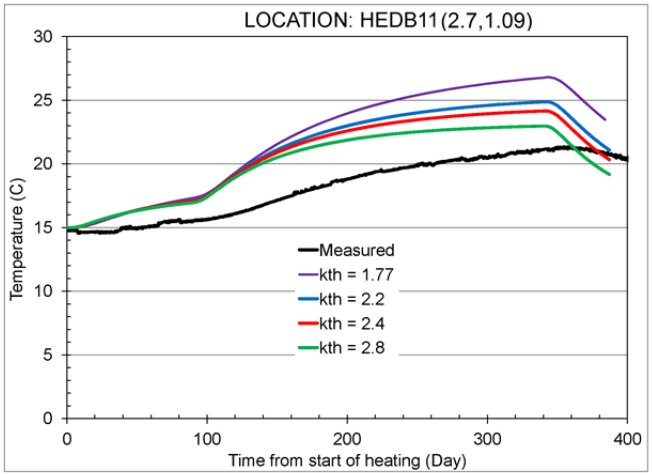

Figure 3-2. Temperature Histories at Locations With Greater Bed-Parallel Than Bed-Normal Distance From the Heater Borehole, Showing the Effects of Thermal Conductivity (k_{th}). Coordinates in Parenthesis are the Bed-Parallel and Bed-Normal Distances (m) Shown in Figure 2-6. [°F = (1.8 × T °C + 32, 1 m = 3.28 ft]

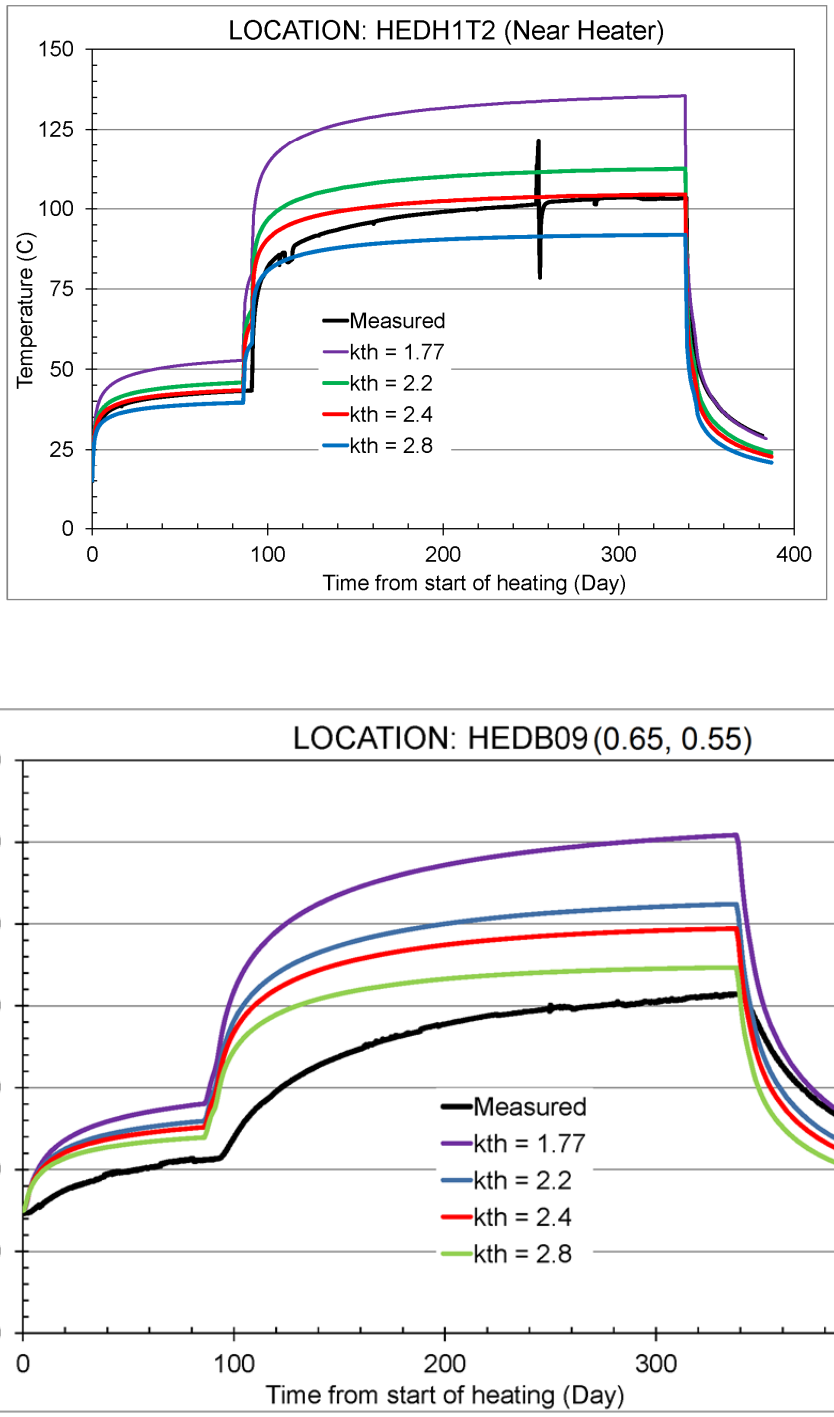

Figure 3-3. Temperature Histories at a Borehole Wall Location Near the Heater and at Location B09 With Approximately Equal Bed-Normal and Bed-Parallel Distances From the Heater Borehole. Coordinates in Parenthesis are the Bed-Parallel and Bed-Normal Distances (m) Shown in Figure 2-6. [°F = (1.8 × T °C + 32) , 1 m = 3.28 ft]

In contrast, temperature histories plotted in Figure 3-2 indicate that the measured temperature histories for the monitored locations shown in the figure are matched better using models with greater thermal conductivity. The monitored locations shown in Figure 3-2 are at a greater bed-parallel than bed-normal distance from the heater. The effective thermal conductivity governing heat transfer from the heater to the locations is influenced more by the bed-parallel than bed-normal conductivity. The results shown in the figure suggest an effective thermal conductivity greater than 2.8 W/m.K for modeling heat flow in this area of the rock mass.

Therefore, the results in Figures 3-1 and 3-2, viewed through the interpretation discussed in the foregoing paragraphs, suggest a bed-normal thermal conductivity smaller than 1.77 W/m.K and a bed-parallel thermal conductivity greater than 2.8 W/m.K for the modeled rock mass. However, because the geometric model used for the analysis (axisymmetric model as described in Figure 2-3) requires an isotropic conductivity and cannot support different bed-normal and bed-parallel conductivities, the authors chose a compromise value of isotropic conductivity.

For estimating the changes in pore water pressure, displacement, and strain in the remainder of this report, a single value of thermal conductivity needed to be selected. Based on the temperature histories in Figure 3-3, which represent locations for the heat transfer in the modeled test that were influenced approximately equally by the bed-normal and bed-parallel conductivities, a value for thermal conductivity of 2.4 W/m.K best represents the rock mass closer to the heat source. The authors acknowledge that there is uncertainty in the proper value to use for an effective thermal conductivity. Considering all three figures (Figures 3-1 through 3-3), all four values of thermal conductivity lead to poor matches for the temperature pattern further from the heat source. Though not discussed further in this report, heterogeneity may be a primary cause for the variations of curves across Figures 3-1 through 3-3. The effect of heterogeneity cannot be calculated at this time. In addition, Gens, et al., (2007) compared results from a 2D axisymmetric model with an isotropic thermal conductivity of 2.2 W/m.K against results from a three-dimensional (3D) anisotropic model with bed-parallel and bed-normal thermal conductivities of 2.8 W/m.K and 1.6 W/m.K, respectively. Gens, et al., (2007) concluded that the difference in temperature calculated using the two models is small and indicates the anisotropy of thermal conductivity may not be significant for the HE-D test. Considering the discussion above, the authors used the value of 2.4 W/m.K to set up the basecase for subsequent analyses in the following subsections.

3.2 Temperature and Pore-Water Pressure Distributions

The calculated temperature distributions (e.g., Figure 3-4) indicate formation of an ellipsoidal heated rock zone, centered in the borehole midway between the heaters. The spatial extent of the heated zone increased as the test proceeded. The shape of the heated zone would most likely differ from the vertical ellipsoid suggested by Figure 3-4 (top plots) because of different bed-normal and bed-parallel thermal conductivities of the rock mass.

A large fraction of the modeled rock volume remained at a temperature below 40 °C [104 °F] through the experiment. Therefore, remobilization of chemically bound water, such as Jobmann, et al. (2006, Figure 4-18) suggested, was likely insignificant in the experiment, if the threshold temperature for the remobilization is approximately 40 °C [104 °F] in Opalinus Clay, as the Jobmann, et al. (2006) data indicated.

The zone of elevated pore-water pressure also is ellipsoidal, but a narrow zone of low pressure occurs within the core of the ellipsoid because of the drainage boundary condition on the heated borehole wall. As the bottom plots of Figure 3-4 show, the point of maximum pore-water

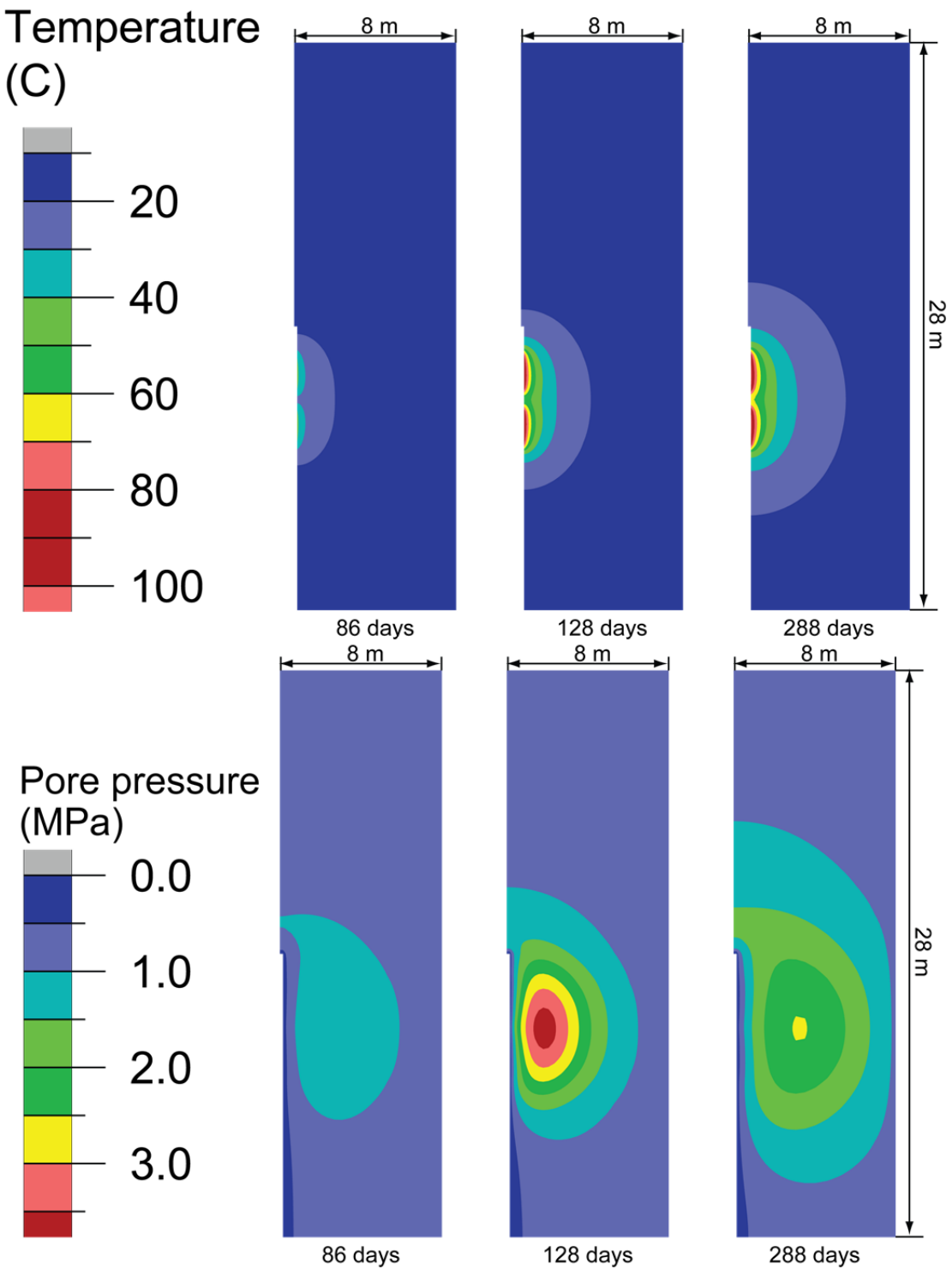

Figure 3-4. Temperature and Pore-Water Pressure Distributions at 86, 128, and 288 Days After the Start of Heating, From CNWRA Basecase Analysis (Table 2-3) [°F = (1.8 × T °C + 32);1 MPa = 145 psi]

pressure occurred at a distance from the borehole and migrated outward from the borehole as the test progressed. This feature of the pore pressure distribution is important because the average hydraulic gradient that drives water flow and dissipation of excess pore pressure at a monitored location is a function of the distance from the point of maximum pore pressure to the monitored location and the distance from the monitored location to the nearest drainage boundary. The driving hydraulic gradient consists of bed-parallel and bed-normal components. The ratio of the bed-parallel to bed-normal hydraulic gradients, which is influenced by anisotropic permeability of the host rock, will affect water flow and pore pressure dissipation at a monitored location, if the bed-parallel and bed-normal permeabilities are different. However, the ratio of the hydraulic gradient components is time-dependent because the peak pore pressure point migrates with time as shown in Figure 3-4. For this reason, any effects of hydrological anisotropy on monitored pore pressures could not be discerned by grouping the monitored locations in terms of the bed-normal and bed-parallel components of distance from the monitored location to the heater borehole. That is, distance from a monitored location to the heater borehole does not have the same significance for pore pressure histories as was shown for the temperature histories in Section 3.1.

3.3 Pore-Water Pressure Histories

In Figures 3-5 and 3-6, the calculated pore pressure histories are compared with the measured pore pressure at the monitored locations. Each figure shows results from five different calculation cases. The parameter combinations for the cases are defined in Table 2-3; except for the case labeled "CNWRA Case with Constant Properties for Liquid Water" in the figures, which is same as that labeled "Basecase 2" in Table 2-2. In Figures 3-5 and 3-6, the plots labeled "D15 Case" and "D15 Case with Full Heat Load" represent analyses performed using a thermal conductivity of 1.77 W/m.K. The other plots represent analyses performed using a thermal conductivity of 2.4 W/m.K. The analysis case "D15 Case with Full Heat Load" is the same as the "CNWRA Basecase" in every respect except for the difference in thermal conductivity. Therefore, these two cases show the effects of thermal conductivity on calculated pore pressure. Smaller thermal conductivity results in greater pore pressure because of greater temperature (see Section 3.1 for the effects of thermal conductivity on temperature). The plots labeled "CNWRA Basecase" and "CNWRA Case with Constant Properties for Liquid Water" illustrate a small change in the calculated pore pressure history by changing liquid water properties to be temperature and pressure dependent as described in Section 2.2. The plot labeled "CNWRA Case with Greater k" shows the effect of permeability on the calculated pore pressure.

Figures 3-7 and 3-8 show the results of additional analyses performed to explore the effects of permeability. As the figures show, the calculated pore pressure buildup increases as the permeability is decreased. The inverse relationship is expected because changes in permeability, which is the ability to transmit perturbations away from a source, inversely affect changes to the gradient. Because increases in permeability lead to a smaller pore pressure buildup, the rate of post-peak dissipation of pore pressure decreases (i.e., post-peak part of the history plot becomes flatter) as the permeability is increased. The figures illustrate the effect of changing the permeability from the base value of 5×10^{-20} m^2 to 2.5×10^{-20}, 1×10^{-19}, and 5×10^{-19} m^2. As the figures show, small changes in permeability could considerably change the calculated pore pressure history. The relationship between the calculated and measured pore pressure in the upper right and lower left plots in Figure 3-8 suggests that a model which includes different values of bed-normal and bed-parallel permeability explicitly could match the measured pore pressure better. The calculated pore pressure from such a model can be increased by reducing the bed-normal permeability and the post-peak dissipation rate can be

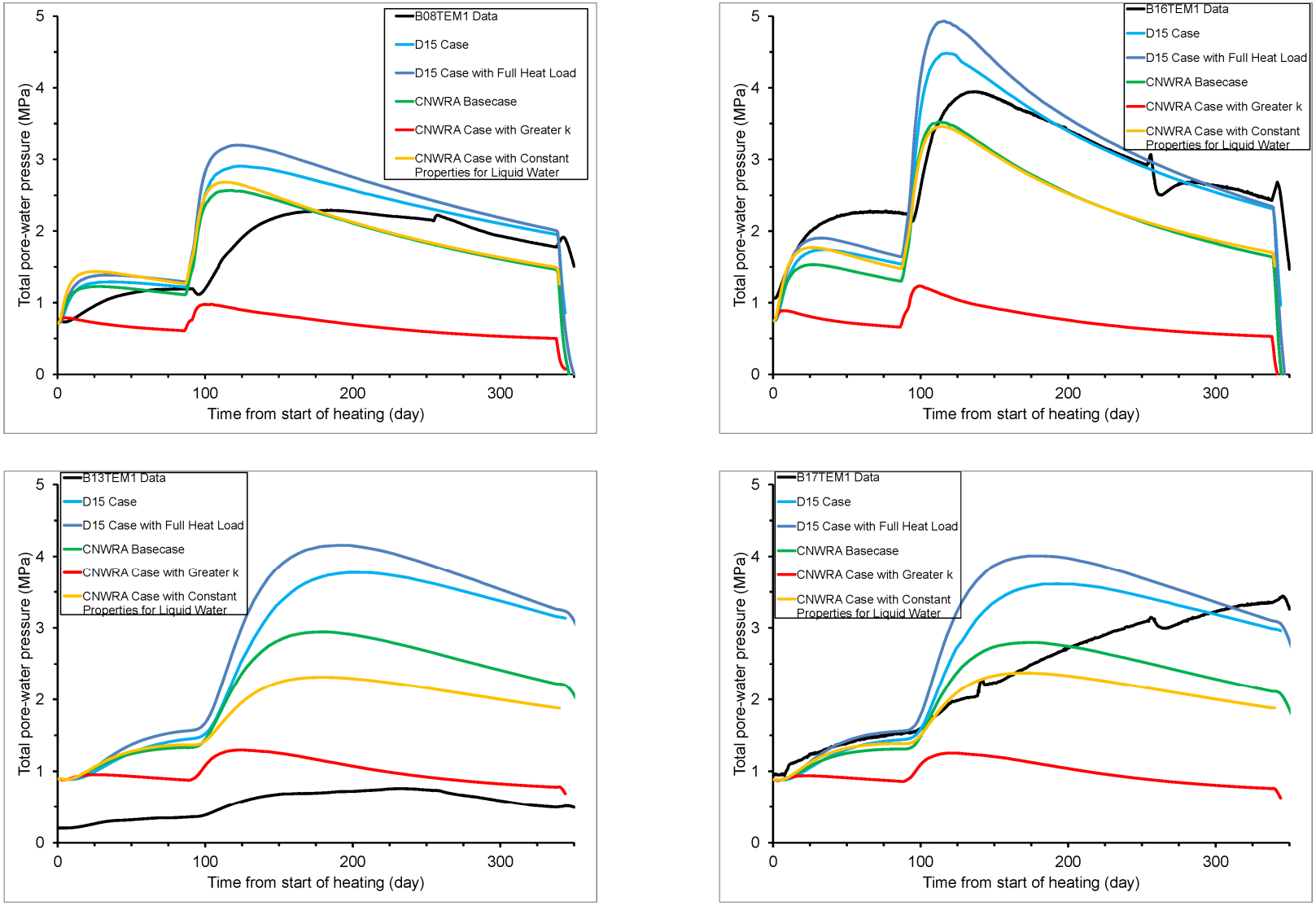

Figure 3-5. Pore Pressure Histories at Locations With Greater Bed-Normal Than Bed-Parallel Distance From the Heater Borehole [1 MPa = 145 psi]

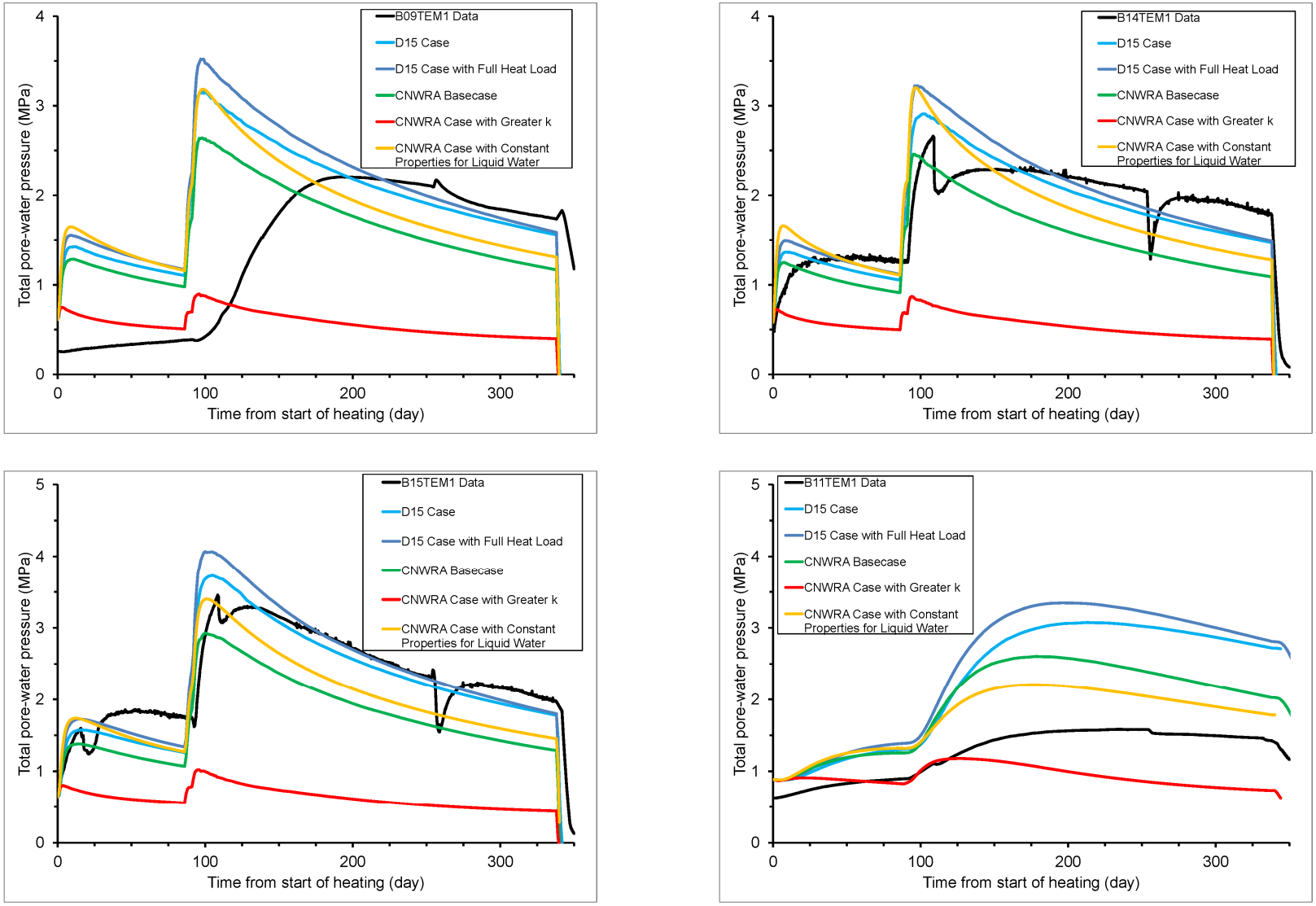

Figure 3-6. Pore Pressure Histories at Locations With Greater Bed-Parallel Than Bed-Normal Distance From the Heater Borehole [1 MPa = 145 psi]

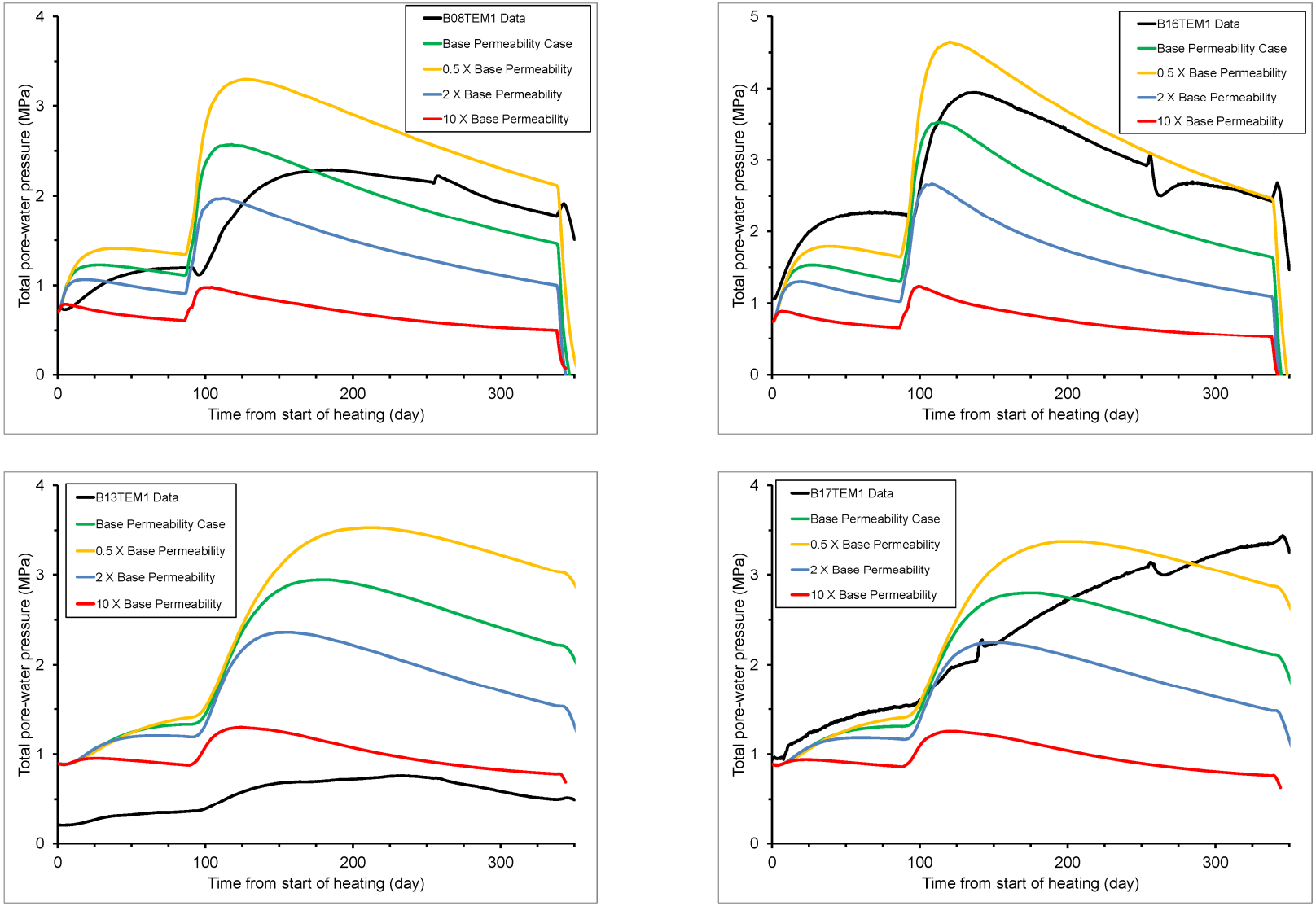

Figure 3-7. Effects of Permeability on Calculated Pore-Pressure Histories for Monitored Locations With Greater Bed-Normal Than Bed-Parallel Distance From the Heater Borehole [1 MPa = 145 psi]

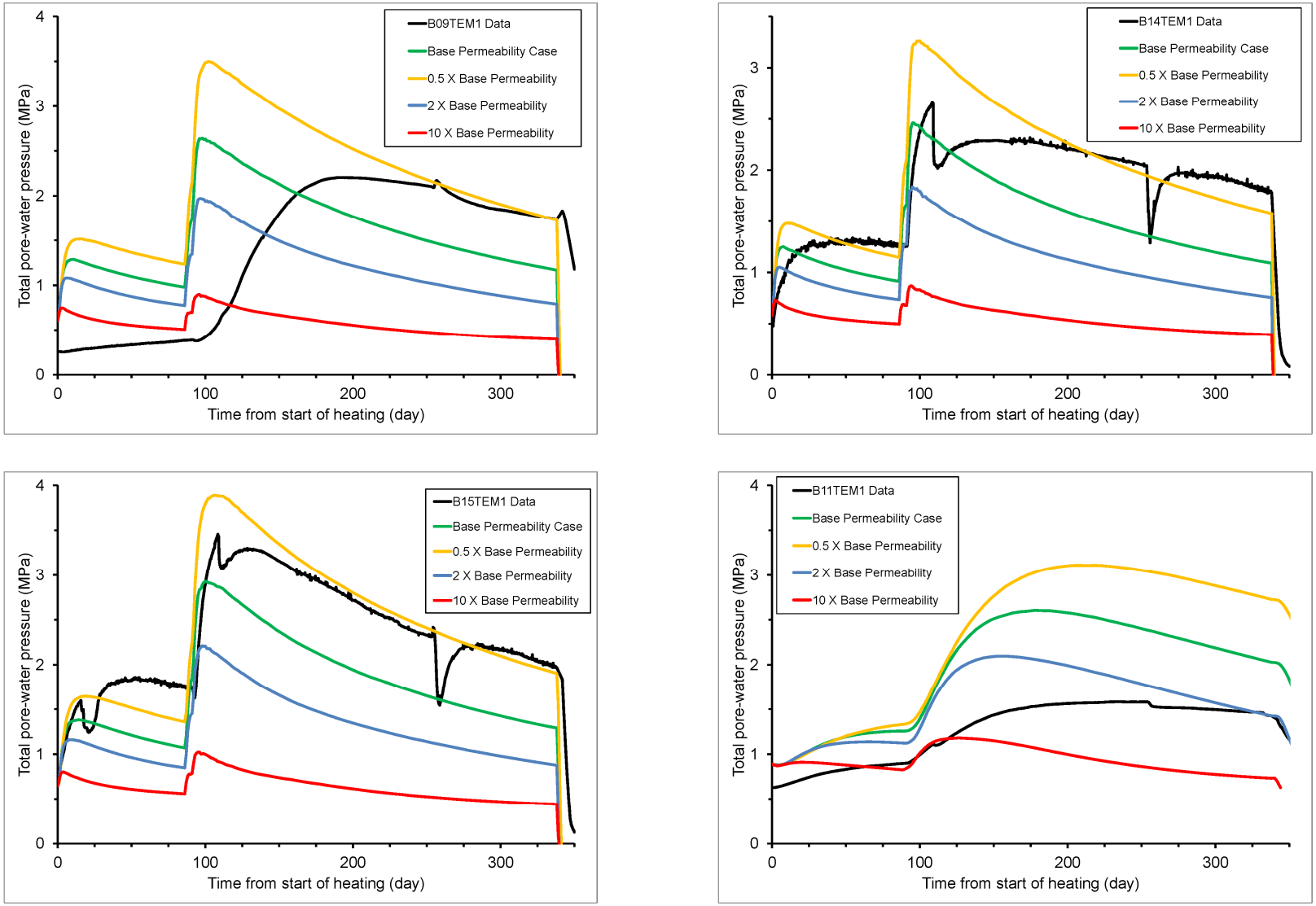

Figure 3-8. Effects of Permeability on Calculated Pore-Pressure Histories for Monitored Locations With Greater Bed-Parallel Than Bed-Normal Distance From the Heater Borehole [1 MPa = 145 psi]

reduced (flattened) by increasing the bed-parallel permeability, relative to the base isotropic permeability value of 5×10^{-20} m^2. These two changes could considerably reduce the differences between the calculated and measured pore pressure in Figures 3-5 through 3-8, though improved details on initial and boundary conditions and thermal parameters would be needed before attempting a better calibration that encompassed all the measurement locations.

Several other considerations may contribute to the poor match at some of the locations (e.g., lower right plots in Figures 3-7 and 3-8). One, measuring equipment not reaching a saturated state before use may have contributed to the difference between the calculated and measured pore pressure. Wileveau and Rothfuchs (2007) suggested that some of the pore-pressure monitors had not attained saturation before the early measurements. Unsaturated monitors may explain the relatively low initial (preheating) pore pressure reflected in the measured pore pressure curves for locations B09 and B13.

Two, the approach used in FLAC for simulating thermally induced pore pressure may have caused some differences between the calculated and measured pore pressure. In geomechanical modeling (such as implemented in FLAC), the increment of pore pressure due to temperature change is proportional to the product $\beta_w K_w(\Delta T)$, where ΔT is the temperature increment and $\beta_w K_w$ is either constant or varies with temperature as shown in Figure 2-8 (lower-right plot). The calculated temperature histories for location B09 (Figure 3-6, upper-left plot) and a few others suggest that this approach may result in a peak pore pressure and postpeak dissipation rate that are too large. The approach could be evaluated further by comparing it with calculated pore pressure histories from thermal-hydrology modeling, such as that implemented in TOUGH, where the pore-pressure is calculated using water properties (e.g., density, viscosity, saturated vapor pressure and specific enthalpy) from the NIST Steam Tables (Pruess, et al., 2012). The two approaches should give similar results, but the incremental approach (applied in geomechanical modeling) could be more sensitive to grid density and time incrementation.

The third consideration is that the difference between the shapes of the calculated and measured pore pressure histories during the constant-temperature periods could suggest occurrence of an additional hydrological process during the period, adding to the pore pressure or delaying dissipation of excess pore pressure. In the areas where temperatures increased above 40 C, remobilization of chemically bound water, such as Jobmann, et al. (2006, Figure 4-18) noted, could suggest such a process if the prevailing temperature for the period supported the remobilization.

3.4 Displacement and Strain Histories

Rock deformation (displacement) was monitored using extensometers B04 and B05 (Figure 3-9). Each extensometer was anchored at the MI niche, and extensometer displacements relative to the anchor were measured periodically at the locations labeled PT01, PT02, and so on along each extensometer (Figure 3-9). The relative displacement is equal to the rock deformation in the extensometer direction at the monitored location. The Task B1 team in the DECOVALEX-2015 project chose the following sign convention: the deformation is positive if directed toward the heater and negative if the opposite direction. The rock deformation also is described in terms of the relative deformation between adjacent monitored locations along an extensometer, referred to as strain and defined as follows

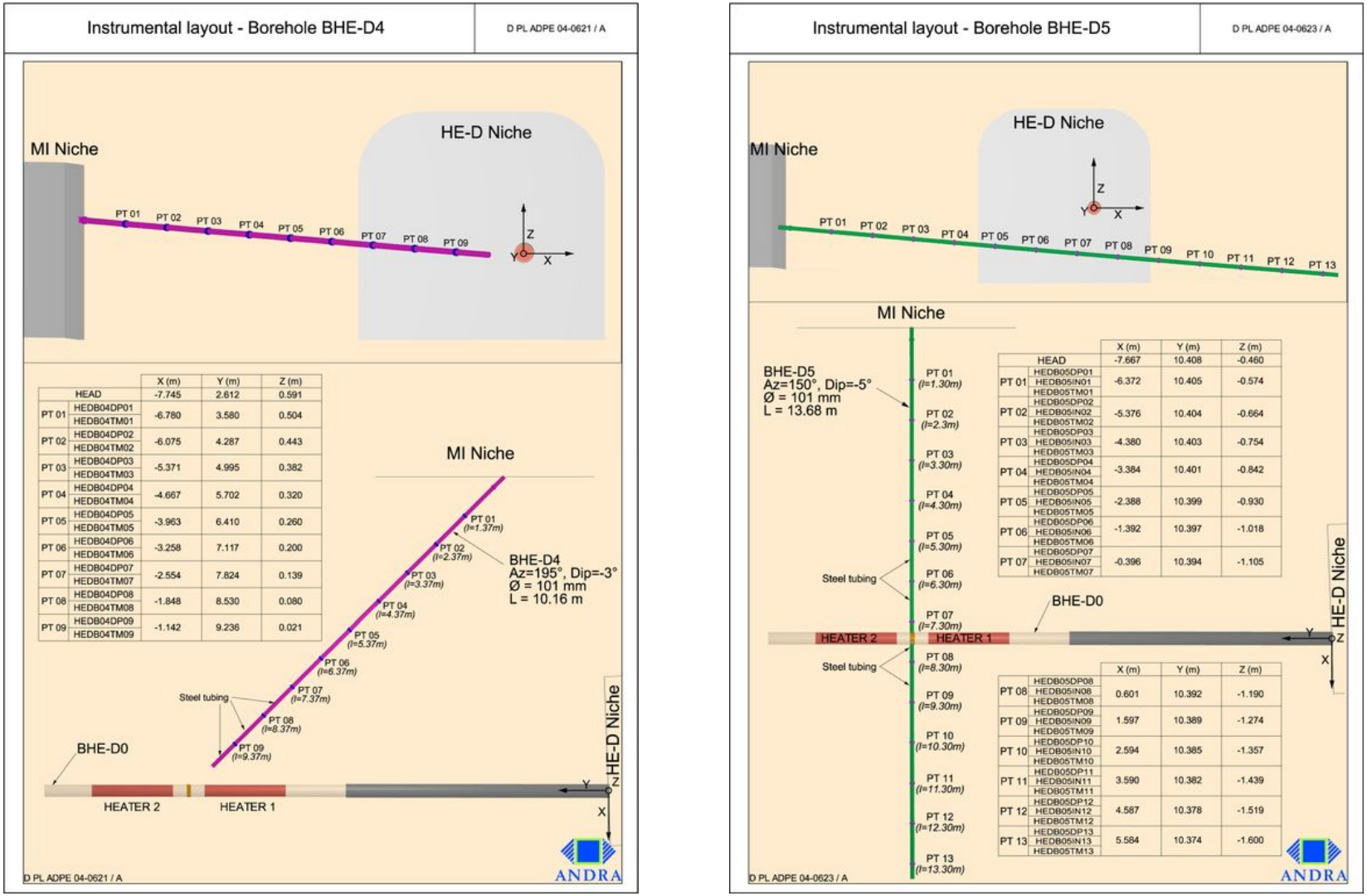

		X (m)	Y (m)	Z (m)
	HEAD	-7.745	2.612	0.591
PT 01	HEDB04DP01 / HEDB04TM01	-6.780	3.580	0.504
PT 02	HEDB04DP02 / HEDB04TM02	-6.075	4.287	0.443
PT 03	HEDB04DP03 / HEDB04TM03	-5.371	4.995	0.382
PT 04	HEDB04DP04 / HEDB04TM04	-4.667	5.702	0.320
PT 05	HEDB04DP05 / HEDB04TM05	-3.963	6.410	0.260
PT 06	HEDB04DP06 / HEDB04TM06	-3.258	7.117	0.200
PT 07	HEDB04DP07 / HEDB04TM07	-2.554	7.824	0.139
PT 08	HEDB04DP08 / HEDB04TM08	-1.848	8.530	0.080
PT 09	HEDB04DP09 / HEDB04TM09	-1.142	9.236	0.021

		X (m)	Y (m)	Z (m)
	HEAD	-7.667	10.408	-0.460
PT 01	HEDB05DP01 / HEDB05IN01 / HEDB05TM01	-6.372	10.405	-0.574
PT 02	HEDB05DP02 / HEDB05IN02 / HEDB05TM02	-5.376	10.404	-0.664
PT 03	HEDB05DP03 / HEDB05IN03 / HEDB05TM03	-4.380	10.403	-0.754
PT 04	HEDB05DP04 / HEDB05IN04 / HEDB05TM04	-3.384	10.401	-0.842
PT 05	HEDB05DP05 / HEDB05IN05 / HEDB05TM05	-2.388	10.399	-0.930
PT 06	HEDB05DP06 / HEDB05IN06 / HEDB05TM06	-1.392	10.397	-1.018
PT 07	HEDB05DP07 / HEDB05IN07 / HEDB05TM07	-0.396	10.394	-1.105
PT 08	HEDB05DP08 / HEDB05IN08 / HEDB05TM08	0.601	10.392	-1.190
PT 09	HEDB05DP09 / HEDB05IN09 / HEDB05TM09	1.597	10.389	-1.274
PT 10	HEDB05DP10 / HEDB05IN10 / HEDB05TM10	2.594	10.385	-1.357
PT 11	HEDB05DP11 / HEDB05IN11 / HEDB05TM11	3.590	10.382	-1.439
PT 12	HEDB05DP12 / HEDB05IN12 / HEDB05TM12	4.587	10.378	-1.519
PT 13	HEDB05DP13 / HEDB05IN13 / HEDB05TM13	5.584	10.374	-1.600

Figure 3-9. Instrument Layout for the HE-D Test Showing the Location of Extensometers B04 (BHE-D4) and B05 (BHE-D5) Relative to the Heater Borehole. Extensometer Locations Monitored for Displacement Are Labeled PT01, PT02, and so on (Wileveau and Rothfuchs, 2007) [1 m = 3.28 ft]

$$e_{bi} = \frac{u_{bi} - u_{b(i-1)}}{l} \tag{3-1}$$

where e_{bi} and u_{bi} are the strain and deformation, respectively, at monitored location PT_i l is the distance between PT_i and $\mathrm{PT}_{(i-1)}$, $i = 1, 2, 3 \cdots \mathrm{etc}$ and PT_0 represents the extensometer anchor.

Strain was calculated for locations PT01 through PT09 on extensometer B04. However, because the calculation model is axisymmetric as described in Section 2, strain was calculated only for locations PT01 through PT07 on extensometer B05. The calculated strains (Figure 3-10, right-side plots) indicate that the first heating stage (i.e., first 100 days of heating, compare with Figure 2-4) had negligible mechanical effects on the rock relative to the subsequent heating stage. Rock deformation was much greater during the second heating stage (days 100 through about 350) and consisted mainly of expansion as the calculated strains indicate, except close to the heated borehole where rock deformation was compressive (compressive strains were calculated for location PT09 on extensometer B04 and locations PT06 and PT07 on extensometer B05).

The measured strains [calculated from measured displacements using Eq. (3-1)] along extensometers B04 and B05 are shown in Figure 3-11. Compared to the calculated (simulated) strains (Figure 3-10, right-side plots), the magnitude of measured strains (Figure 3-11) is generally greater than the calculated strains. Also, whereas the calculated results indicate the rock in compression near the heat source and extension away from the heat source, the measured strains indicate a more complex mix of extensional and compressive deformations within the rock between the heat source and the MI niche. Although the calculated strains could be modified by adjusting the mechanical parameters, the authors focused on adjusting the thermal and hydrological parameters to obtain calculated temperatures and pore pressures that match the measured temperatures and pore pressures as closely as possible. The mechanical parameters would have been adjusted if necessary after the authors were satisfied with the calculated thermal and hydrological response. The mechanical parameters were not adjusted, because, as explained in Sections 3.1 and 3.3, the model geometry would have been changed to allow explicit representation of different bed-normal and bed-parallel thermal and hydraulic conductivities in order to achieve calculated temperature and pore pressure that match the measurements better. The authors decided against the model change with the expectation that the understanding of the thermal-hydrological behavior of the rock (described in Sections 3.1 through 3.3) is sufficient to model the HE-E test, which is the main objective of Task B1 (as explained in Chapter 1). The relevant hydrothermal parameters indicated from the HE-D modeling could be used as a starting point for calibration for the HE-E test.

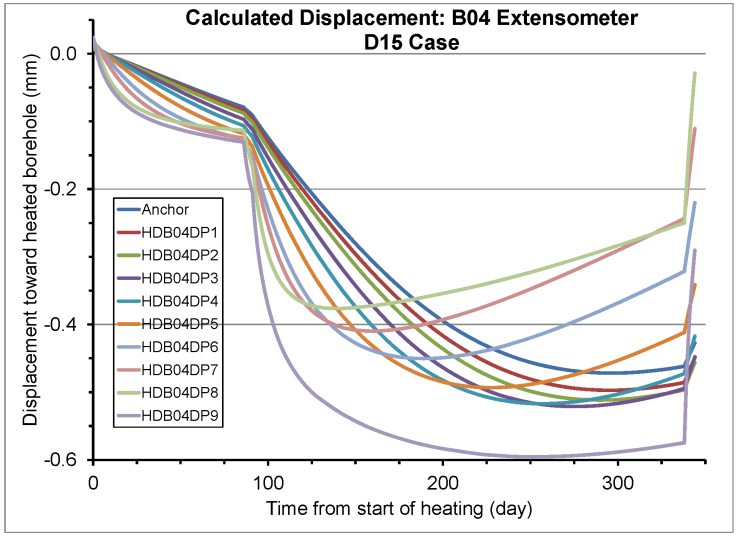

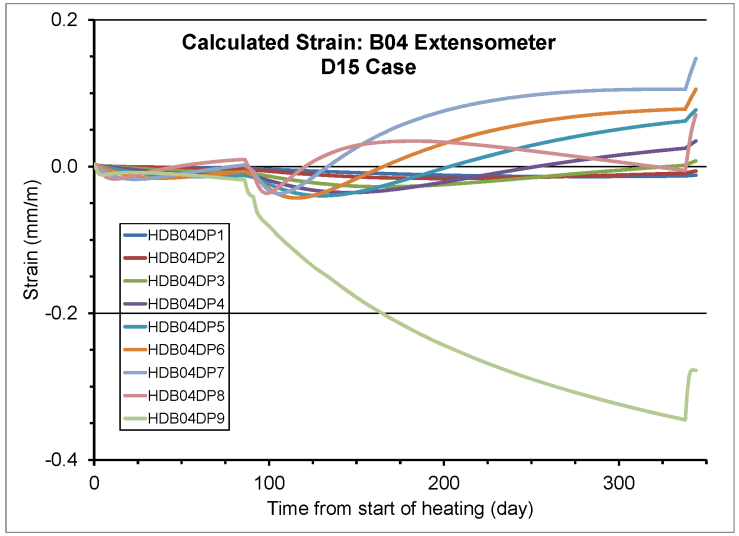

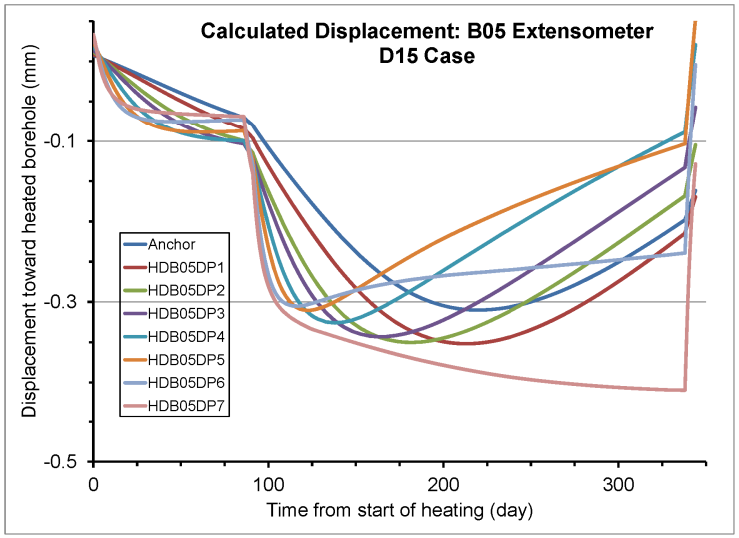

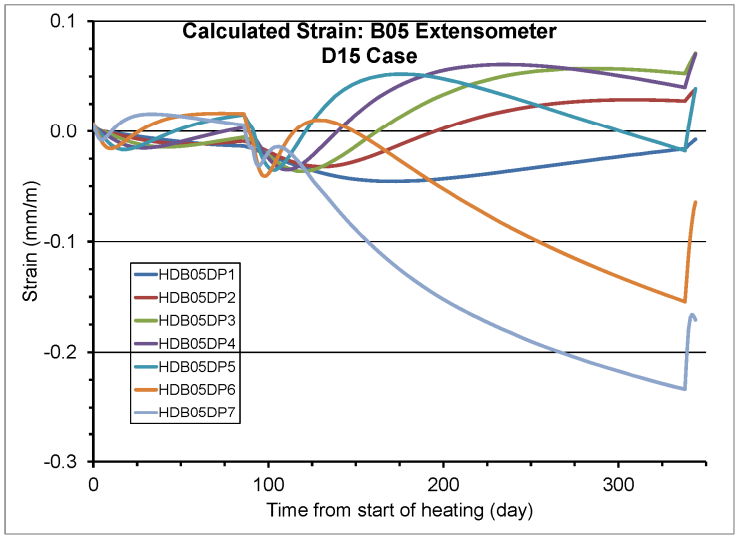

Figure 3-10. Calculated Rock Deformation (Displacement) and Strain Along Extensometers B04 and B05 From D15 Case in Table 2-3. Deformation is Positive Toward the Heater Borehole and Extensional Strain is Positive. [1 mm = 0.04 in]

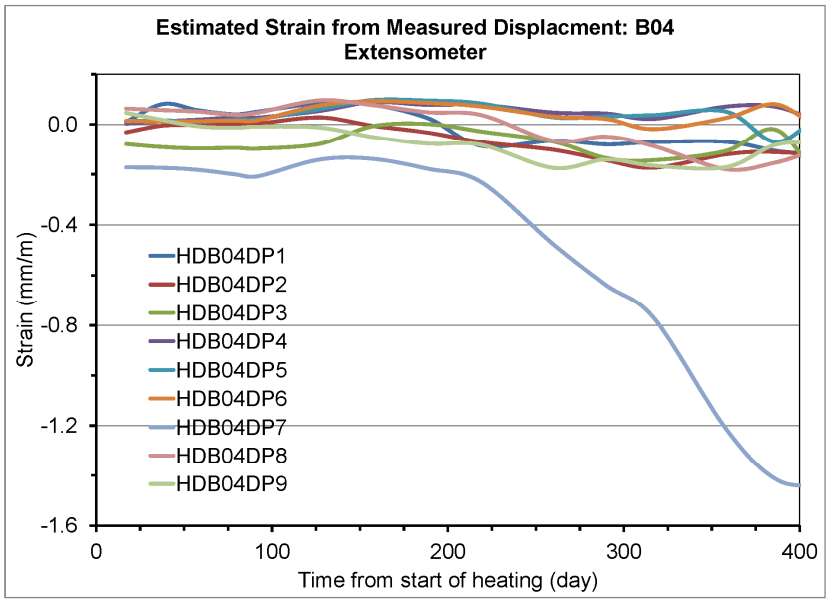

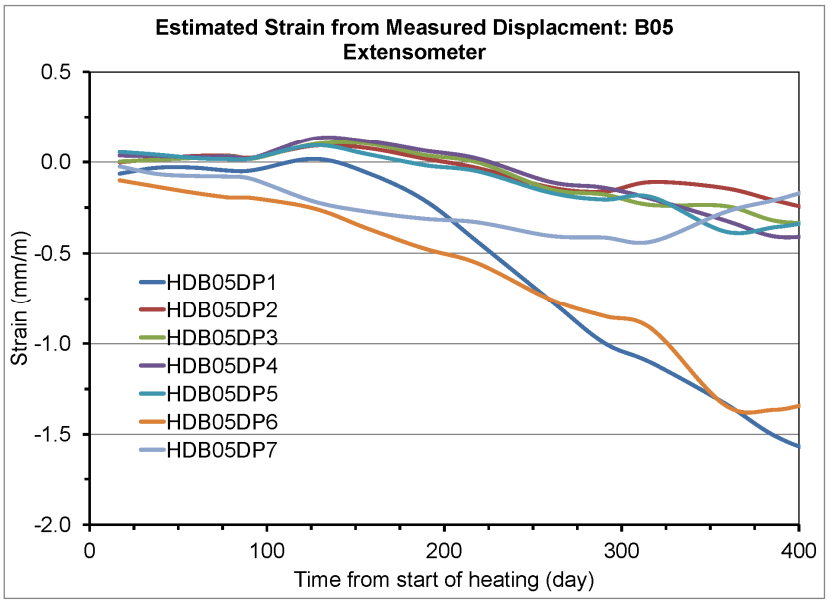

Figure 3-11. Measured Rock Strain Along Extensometers B04 and B05. Extensional Strain is Positive.

4 SUMMARY

Task B1 in the current phase of DECOVALEX (D-2015) focuses on understanding THM processes in bentonite buffer and argillaceous host rock (Opalinus Clay) based on field tests at Mont Terri URL in Switzerland. Modeling the THM processes in the Opalinus Clay, as observed in the HE-D heater test, was the first step of Task B1 and was the focus of this report. Opalinus Clay is a stiff, layered, Mesozoic clay of marine origin. Temperature, pore-pressure, and rock strain were monitored in several locations in the heated borehole and the rock. The HE-D test involved heating the rock in two stages. The first heating stage was for 90 days at a power of 650 W. The power was increased to 1,950 W during the second heating stage for 248 days after which the power was turned off. The cool-down phase was monitored for 7 months. The important THM processes include heat conduction through the rock, thermal expansion of the rock and pore fluid, thermally induced pore pressure generation, time-dependent dissipation of excess pore pressure, and rock deformation caused by these processes. The FLAC code was considered well suited for modeling these processes.

A 2D axisymmetric model {8 × 28 m [26 × 92 ft]} centered on the axis of the heated borehole was set up with THM boundary conditions consistent with the conditions at a radial distance of 8 m [26 ft] from the borehole axis. Most of the input parameters were based on previously published reports and journal articles. The THM processes were coupled sequentially by using the output from a thermal calculation to drive the hydrological calculation and using results of the TH calculations to drive the mechanical calculation. Time incrementation was controlled by the thermal calculation and the exchange of input and output among the THM calculations was implemented using user-defined functions based on the FISH language in FLAC. The FISH functions also accounted for changes in water properties (e.g., density, thermal expansivity, bulk modulus, and viscosity) in response to temperature. The calculated results were used to evaluate temperature and pore-pressure response to imposed heat load. The mechanical response was also described in terms of the calculated rock deformation but did not receive as much emphasis as the thermal and hydrological responses. The calculated results are consistent with the conceptualization of the TH behavior (i.e., the thermal load drives an increase in rock temperature that in turn drives a pore-pressure increase, and the dissipation of excess pore pressure is driven by a hydraulic gradient defined by the distribution of excess pore pressures and drainage boundary conditions).

The calculated results for temperature generally capture the evolution of temperatures at several monitored locations in response to the heating and cool-down phases. Temperature contour plots indicate a formation of an ellipsoidal heated rock zone that expanded as the test progressed. Analysis of the calculated and measured temperature histories indicates that a thermal conductivity anisotropy defined in terms of a difference between the bed-normal and bed-parallel thermal conductivity likely affected the measured temperature significantly. A sensitivity analysis of the effects of thermal conductivity on the calculated temperature suggests a bed-normal thermal conductivity less than 1.77 W/m.K and a bed parallel thermal conductivity greater than 2.8 W/m.K.

The calculated results also show an ellipsoidal zone of elevated pore pressure. The point of maximum pore pressure migrated outwards from the borehole as the test progressed. The calculated pore pressures were sensitive to the thermal conductivity, with smaller thermal conductivity values resulted in higher pore pressures, consistent with a smaller thermal conductivity, resulting in greater temperature and, therefore, greater pore pressure. The pore pressures were sensitive to permeability of the rock. Calculated pore pressure increased as permeability decreased. The sensitivity of calculated pore pressure to permeability suggests

that a permeability anisotropy defined in terms of a difference between the bed-normal and bed-parallel permeability likely contributed to the trends in measured pore pressure.

Calculated deformations indicate that the first heating stage had a negligible mechanical effect on the rock relative to the second heating stage. The results indicate that the rock mass expanded during the second heating stage. Generally, the amount of expansion increased with distance from the heater to a maximum value and decreased with distance thereafter.

Developing a numerical model for the HE-D heater test at Mont Terri provided an in-depth understanding of THM behavior of the Opalinus Clay. The results of this study indicate that the anisotropy of thermal and hydrological properties (i.e., thermal and hydraulic conductivities in bed-parallel directions differ from the bed-normal conductivities) likely play an important role in the THM processes in the Opalinus Clay. This conclusion will be evaluated in the context of the HE-E test that focuses on THM behavior of the buffer and its interaction with the host rock.

5 REFERENCES

Garitte, B. "General Discussions (Task B1)." Presentation at the Workshop 3 DECOVALEX 2015, Jeju Island, South Korea, April 16, 2013. Stockholm, Sweden: Royal Institute of Technology. 2013.

Garitte, B., A. Bond, A. Millard, C. Zhang, C. McDermott, S. Nakama, and A. Gens. "Analysis of Hydro-Mechanical Processes in a Ventilated Tunnel in an Argillaceous Rock on the Basis of Different Modelling Approaches." *Journal of Rock Mechanics and Geotechnical Engineering.* Vol. 5, Issue 1. pp. 1–17. 2013.

Garitte, B., J. Vaunat, and A. Gens. "HE-D Experiment: Thermohydromechanical Modelling of the HE-D Experiment at Mont-Terri (Switzerland)." Technical Note 2006-44. Barcelona, Spain: Universitat Politècnica De Catalunya. 2007.

Gaus, I., K. Wieczorek, K. Schuster, B. Garitte, R. Senger, R., Vasconcelos and J. C. Mayor "EBS Behaviour Immediately After Repository Closure in a Clay Host Rock: HE-E Experiment (Mont Terri URL)". Geological Society. London. Special Publications. Doi 10.1144/SP400.11. 2014.

Gens, A., J. Vaunat, B. Garitte, and Y. Wileveau. "*In-Situ* Behaviour of a Stiff Layered Clay Subject to Thermal Loading: Observations and Interpretation." *Geotechnique*. Vol. 57, No. 2. pp. 207–228. 2007.

Itasca Consulting Group. "FLAC V 7.0, Fast Lagrangian Analysis of Continua, User's Guide." Minneapolis, Minnesota: Itasca Consulting Group. 2011

Jobmann, M., M. Polster, and M. Schonebeck. "Investigation on Thermal Expansion Effects in Clay Formations—TEE—Final Report." Peine, Germany: DBE Technology. 2006.

Pruess, K., C. Oldenburg, and G. Moridis. "TOUGH2 User's Guide Version 2.0." LBNL–43134. Berkeley, California: Lawrence Berkeley National Laboratory.
p. 198. 2012.

NIST (National Institute of Standard Technology). "Thermophysical Properties of Fluid System." 2011. <http://webbook.nist.gov/chemistry/fluid> (8 August 2013).

UPC. "HE-D Experiment: Thermohydromechanical Modelling of the HE-D Experiment at Mont-Terri (Switzerland)." Technical Note 2006–44. Barcelona, Spain: Universitat Politècnica De Catalunya. 2007.

Wileveau, Y. "THM Behaviour of Host Rock: (HE-D Experiment): Progress Report September 2003–October 2004." Mont Terri Project TR 2005-03. Sceaux, France: ANDRA. 2005.

Wileveau, Y. and T. Rothfuchs. "THM Behaviour of Host Rock (HE-D) Experiment: Study of Thermal Effects on Opalinus Clay." Mont Terri Project TR 2006-01. Sceaux, France: ANDRA. 2007.

Zhang, C.-L., T. Rothfuchs, N. Jockwer, K.L. Wieczorek, J. Tittrich, J. Müller, L. Hartwig, and M. Komischke. “Thermal Effects on the Opalinus Clay: A Joint Heating Experiment of ANDRA and GRS at the Mont Terri URL (HE-D Project).” TR 2007-02. Berlin, Germany: Gesellschaft für Anlagenund Reaktorsicherheit (GRS) mbH. 2007.

APPENDIX A

LAYOUT INFORMATION

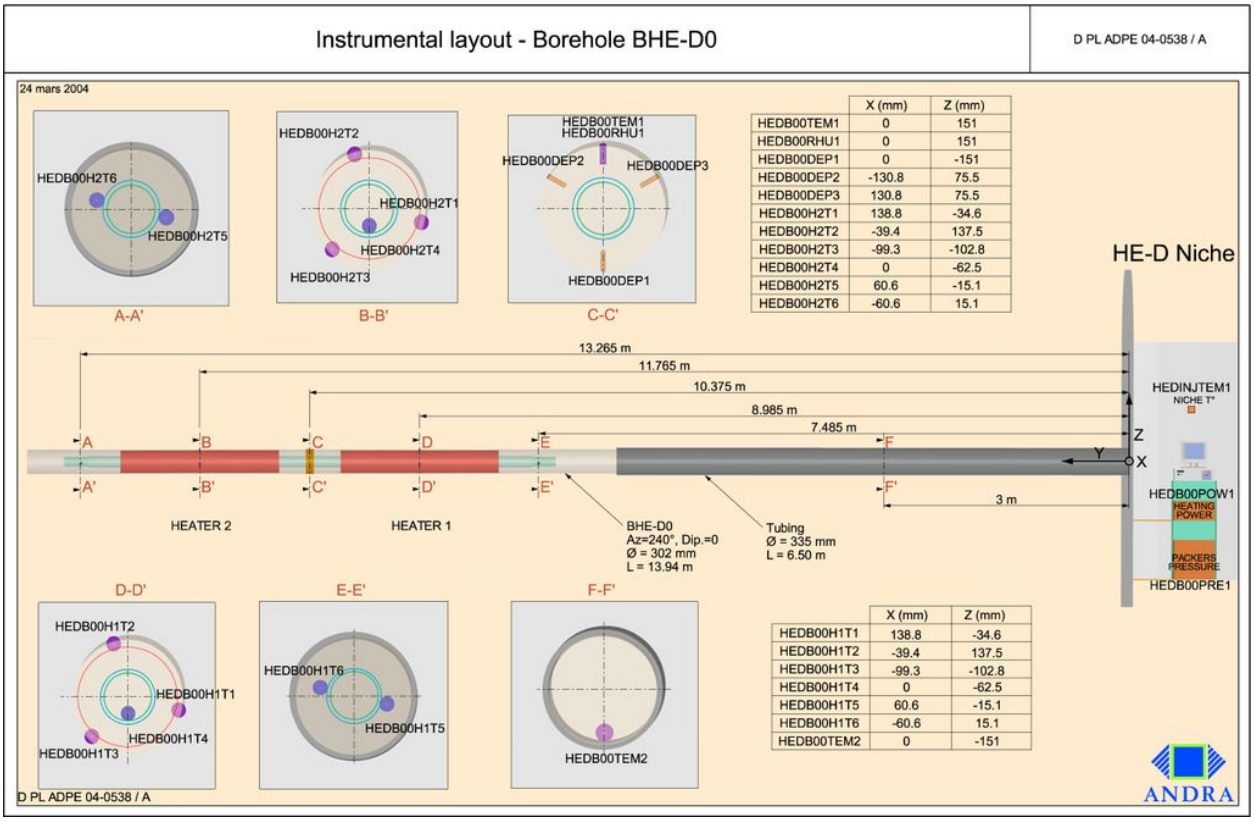

	X (mm)	Z (mm)
HEDB00TEM1	0	151
HEDB00RHU1	0	151
HEDB00DEP1	0	-151
HEDB00DEP2	-130.8	75.5
HEDB00DEP3	130.8	75.5
HEDB00H2T1	138.8	-34.6
HEDB00H2T2	-39.4	137.5
HEDB00H2T3	-99.3	-102.8
HEDB00H2T4	0	-62.5
HEDB00H2T5	60.6	-15.1
HEDB00H2T6	-60.6	15.1

	X (mm)	Z (mm)
HEDB00H1T1	138.8	-34.6
HEDB00H1T2	-39.4	137.5
HEDB00H1T3	-99.3	-102.8
HEDB00H1T4	0	-62.5
HEDB00H1T5	60.6	-15.1
HEDB00H1T6	-60.6	15.1
HEDB00TEM2	0	-151

Figure A–1. Layout of the HED Heater Borehole (D0)
(Wileveau and Rothfuchs, 2007, Figure 2-6)

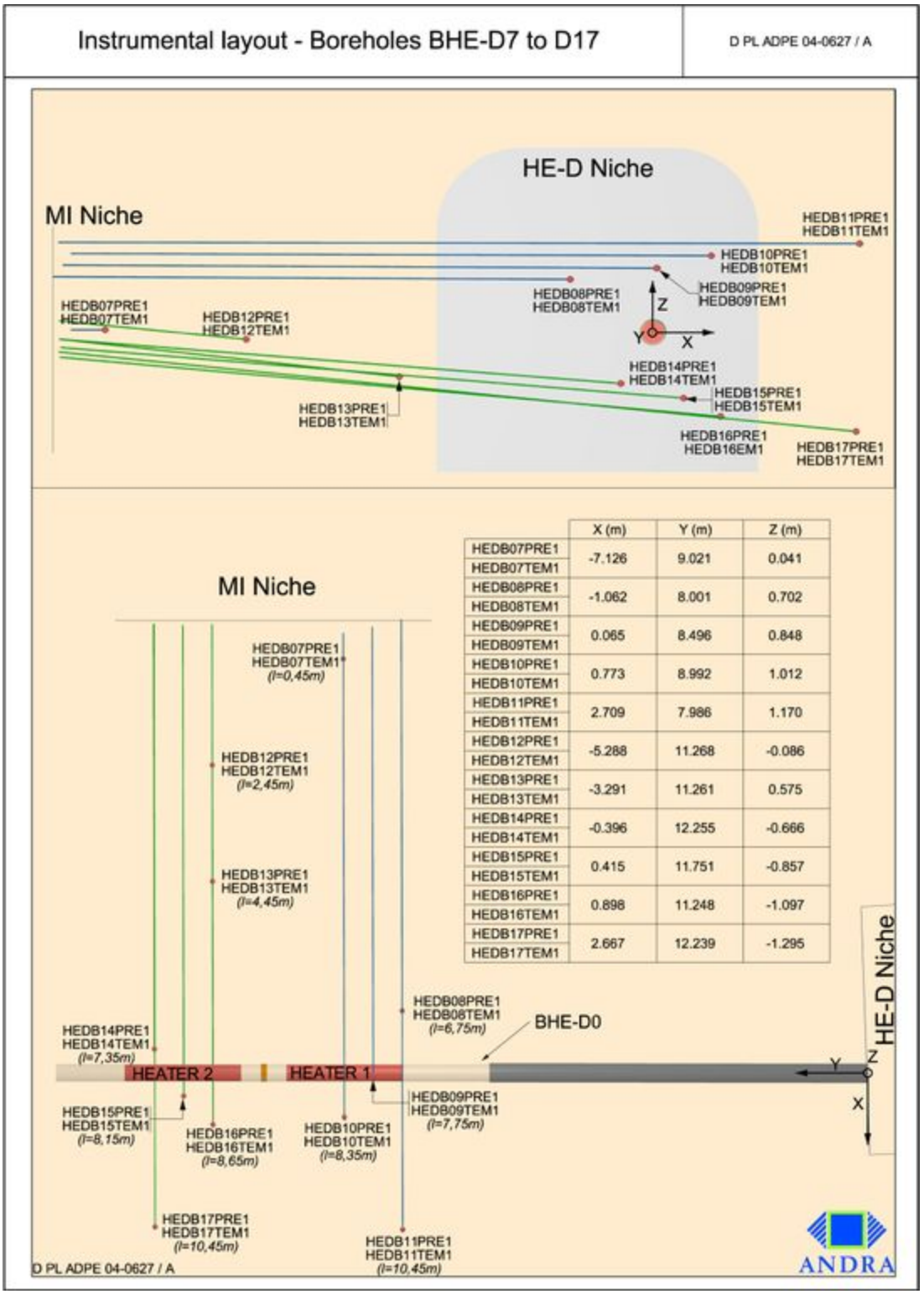

	X (m)	Y (m)	Z (m)
HEDB07PRE1	-7.126	9.021	0.041
HEDB07TEM1			
HEDB08PRE1	-1.062	8.001	0.702
HEDB08TEM1			
HEDB09PRE1	0.065	8.496	0.848
HEDB09TEM1			
HEDB10PRE1	0.773	8.992	1.012
HEDB10TEM1			
HEDB11PRE1	2.709	7.986	1.170
HEDB11TEM1			
HEDB12PRE1	-5.288	11.268	-0.086
HEDB12TEM1			
HEDB13PRE1	-3.291	11.261	0.575
HEDB13TEM1			
HEDB14PRE1	-0.396	12.255	-0.666
HEDB14TEM1			
HEDB15PRE1	0.415	11.751	-0.857
HEDB15TEM1			
HEDB16PRE1	0.898	11.248	-1.097
HEDB16TEM1			
HEDB17PRE1	2.667	12.239	-1.295
HEDB17TEM1			

Figure A–2. Layout of the Pore-Water Pressure and Temperature Sensors Installed in Boreholes D07 to D17 (Wileveau and Rothfuchs, 2007, Figure 2-12)

REFERENCE

Wileveau, Y. and T. Rothfuchs. "THM Behaviour of Host Rock (HE-D) Experiment: Study of Thermal Effects on Opalinus Clay." Mont Terri Project TR 2006-01. Sceaux, France: ANDRA. 2007.

APPENDIX B

MONITORING LOCATION COORDINATES

Table B–1. Coordinates of the Monitoring Locations								
Parameters Monitored	**Monitoring Locations**	**Original Coordinates (m)**			**Modified Radial Coordinates (m)**		**Bed Parallel Coordinates (BPC)**	**Bed Normal Coordinates (BNC)**
		x	y	z	r	h		
Temperature	HEDB00H1T2	0.0394	8.985	0.1375	0.14	8.99	—	—
Temperature and Pore Pressure	HDB08TEM1	1.062	8.001	0.702	1.27	8.00	0.25	1.25
Temperature and Pore Pressure	HDB09TEM1	−0.065	8.496	0.848	0.85	8.50	0.65	0.55
Temperature and Pore Pressure	HDB10TEM1	−0.773	8.992	1.012	1.27	8.99	1.26	0.17
Temperature and Pore Pressure	HDB11TEM1	−2.709	7.986	1.17	2.95	7.99	2.74	1.09
Temperature and Pore Pressure	HDB13TEM1	3.291	11.261	0.575	3.34	11.26	1.92	2.73
Temperature and Pore Pressure	HDB14TEM1	0.396	12.255	−0.666	0.77	12.26	0.75	0.19
Temperature and Pore Pressure	HDB15TEM1	0.415	11.751	−0.857	0.95	11.75	0.90	0.31
Temperature and Pore Pressure	HDB16TEM1	−0.898	11.248	−1.097	1.42	11.25	0.14	1.41
Temperature and Pore Pressure	HDB17TEM1	−2.667	12.239	−1.295	2.96	12.24	0.97	2.80

$r = \sqrt{x^2 + z^2}$
$h = y$
$BPC = |(x\cos\theta + z\sin\theta)|$; $BNC = |(-x\sin\theta + z\cos\theta)|$ where $\theta = 45°$
1 m = 3.28 ft